

RESEARCH ARTICLE

Piezo1 regulates calcium oscillations and cytokine release from astrocytes

María Velasco-Estevez¹ | Sara O. Rolle^{2,3} | Myrthe Mampay⁴ | Kumlesh K. Dev¹  | Graham K. Sheridan^{4,5} ¹Drug Development, Department of Physiology, School of Medicine, Trinity College Dublin, Dublin, Ireland²Department of Bioengineering, Imperial College London, London, UK³Francis Crick Institute, London, UK⁴School of Pharmacy and Biomolecular Sciences, University of Brighton, Brighton, UK⁵School of Life Sciences, Queen's Medical Centre, University of Nottingham, Nottingham, UK**Correspondence**Graham Sheridan, School of Life Sciences, Queen's Medical Centre, University of Nottingham, Nottingham, UK.
Email: graham.sheridan@nottingham.ac.uk**Funding information**

Leverhulme Trust, Grant/Award Number: RPG-2018-443

Abstract

Astrocytes are important for information processing in the brain and they achieve this by fine-tuning neuronal communication via continuous uptake and release of biochemical modulators of neurotransmission and synaptic plasticity. Often overlooked are their important functions in mechanosensation. Indeed, astrocytes can detect pathophysiological changes in the mechanical properties of injured, ageing, or degenerating brain tissue. We have recently shown that astrocytes surrounding mechanically-stiff amyloid plaques upregulate the mechanosensitive ion channel, Piezo1. Moreover, ageing transgenic Alzheimer's rats harboring a chronic peripheral bacterial infection displayed enhanced Piezo1 expression in amyloid plaque-reactive astrocytes of the hippocampus and cerebral cortex. Here, we have shown that the bacterial endotoxin, lipopolysaccharide (LPS), also upregulates Piezo1 in primary mouse cortical astrocyte cultures in vitro. Activation of Piezo1, via the small molecule agonist Yoda1, enhanced Ca^{2+} influx in both control and LPS-stimulated astrocytes. Moreover, Yoda1 augmented intracellular Ca^{2+} oscillations but decreased subsequent Ca^{2+} influx in response to adenosine triphosphate (ATP) stimulation. Neither blocking nor activating Piezo1 affected cell viability. However, LPS-stimulated astrocyte cultures exposed to the Piezo1 activator, Yoda1, migrated significantly slower than reactive astrocytes treated with the mechanosensitive channel-blocking peptide, GsMTx4. Furthermore, our data show that activating Piezo1 channels inhibits the release of cytokines and chemokines, such as IL-1 β , TNF α , and fractalkine (CX₃CL1), from LPS-stimulated astrocyte cultures. Taken together, our results suggest that astrocytic Piezo1 upregulation may act to dampen neuroinflammation and could be a useful drug target for neuroinflammatory disorders of the brain.

Abbreviations: A β 42, amyloid- β 1–42 peptide; BSA, bovine serum albumin; CNS, central nervous system; DMEM, Dulbecco's modified eagle's medium; DMSO, dimethyl sulfoxide; ER, endoplasmic reticulum; FBS, foetal bovine serum; GFAP, glial fibrillary acidic protein; HBSS, Hank's balanced salt solution; HRP, horse radish peroxidase; IL, interleukin; LPS, lipopolysaccharide; PBS, phosphate-buffered saline; PVDF, polyvinylidene difluoride; RIPA, radioimmunoprecipitation assay; RRID, research resource identifier; SDS-PAGE, sodium dodecyl sulfate polyacrylamide gel electrophoresis; TNF α , tumor necrosis factor-alpha.

**KEYWORDS**

astrocytes, calcium oscillations, lipopolysaccharide, mechanosensitive ion channel, Piezo1, pro-inflammatory cytokines

1 | INTRODUCTION

Astrocytes are the most abundant glial cell type in the brain and form interconnected neuron-glia networks that are exquisitely sensitive sensors and modulators of neuronal activity (Copeland et al., 2017; Fellin et al., 2004; Serrano, Haddjeri, Lacaillle, & Robitaille, 2006). Astrocytes are also highly mechanosensitive cells (Blumenthal, Hermanson, Heimrich, & Shastri, 2014; Moshayedi et al., 2010) and can detect changes in the mechanical properties of their surrounding microenvironment during disease of the central nervous system (CNS) or following traumatic injury (Maneshi, Sachs, & Hua, 2015; Moshayedi et al., 2014). We have recently shown that astrocytes, which wrap and engulf stiff amyloid plaques in the ageing rat brain upregulate expression of the mechanosensitive ion channel, Piezo1 (Velasco-Estevez et al., 2018). Piezo1 is a nonselective cation channel expressed on the outer cell membrane and is permeable to extracellular calcium (Ca^{2+}) influx (Gottlieb & Sachs, 2012; Li et al., 2015). The calcium-mediated mechanotransduction signaling cascades activated by Piezo1 channel opening are important in a range of developmental and physiological processes including neuronal differentiation (Pathak et al., 2014), axon guidance (Koser et al., 2016), confinement-sensing and cell migration (Hung et al., 2016), neuronal regeneration (Song et al., 2019), shear stress-mediated vasodilation (Wang et al., 2016), and immune cell activation (Liu et al., 2018). However, the intracellular molecular mechanisms that underlie Piezo1's role in many of the above cellular processes have yet to be fully elucidated. McHugh et al. (2010) have shown that Piezo1 channels localize to the endoplasmic reticulum (ER) in epithelial cells where they can regulate integrin-mediated cell adhesion via calpain and talin activation. Therefore, Piezo1 channels can regulate intracellular Ca^{2+} concentrations via Ca^{2+} release from intracellular stores or through the formation of mechanically-gated ion channels in the outer cell membrane (Nourse & Pathak, 2017). Interestingly, Piezo1 is also voltage sensitive (Moroni, Servin-Vences, Fleischer, Sanchez-Carranza, & Lewin, 2018) and, therefore, its repertoire of known functions in CNS neurons and glial cells, both in health and disease, is likely to increase in the near future.

In endothelial cells, shear stress activates Piezo1-mediated Ca^{2+} influx leading to the release of adenosine triphosphate (ATP; Wang et al., 2016). In turn, ATP can activate purinergic G protein-coupled receptors, such as P2Y_1 and P2Y_2 , on neighboring cells causing the upregulation of nitric oxide synthase (NOS; Jacob, Perez Novo, Bachert, & Van Crombruggen, 2013). Nitric oxide (NO) release from astrocytes acts as an important neuromodulator in the brain and can induce further gliotransmitter release, including glutamate (Bal-Price, Moneer, & Brown, 2002). ATP and glutamate have a wide range of functions at the synapse and can initiate Ca^{2+} oscillations and Ca^{2+} waves in astrocytes (Leybaert & Sanderson, 2012; Scemes & Giaume, 2006), thus modulating

long-range communication and information processing through astrocyte-neuron networks. ATP can also regulate the release of neuromodulators from astrocytes, such as cytokines that fine-tune local neurotransmission and synaptic plasticity processes (Adzic et al., 2017; Nishizaki, 2004). Interestingly, astrocytic Piezo1 expression was relatively high in the cortex and hippocampus of transgenic Alzheimer's rats (TgF344-AD) that harbored a chronic urinary tract infection (UTI) of *Escherichia coli* (*E. coli*). This suggests that raised levels of cytokines, chemokines, and neuroinflammation, which often develops in the elderly as a result of chronic peripheral immune activation (Chesnokova, Pechnick, & Wawrowsky, 2016; Simen, Bordner, Martin, Moy, & Barry, 2011), may lead to the enhanced expression of Piezo1 in amyloid plaque-reactive astrocytes (Velasco-Estevez et al., 2018). However, whether this upregulation of mechanosensitive Ca^{2+} permeable channels in the ageing Alzheimer's disease brain is neuroprotective, or instead enhances neuro-damaging signaling cascades, is as yet unknown.

Here, we used an in vitro murine-derived primary astrocyte culture model to examine the effects of activating Piezo1 on several key functional parameters including (a) cytosolic Ca^{2+} oscillations, (b) ATP-induced Ca^{2+} influx, (c) astrocyte migration, and (d) cytokine and chemokine release from control and LPS-stimulated astrocyte cultures. The aim was to investigate if upregulation of Piezo1 in reactive astrocytes exacerbates neuroinflammation or whether Piezo1 expression in LPS-stimulated astrocytes could be an innate neuroprotective response to disease pathogenesis in the inflamed brain.

2 | MATERIALS AND METHODS

2.1 | Ethics statement

All experiments involving animals, and Schedule 1 protocols used to obtain brain tissue, were approved by the Animal Welfare and Ethical Review Bodies (AWERB committees) of the University of Brighton and Trinity College Dublin. This study was conducted in accordance with the principles of the Basel Declaration and adhered to the legislation detailed in the UK Animals (Scientific Procedures) Act 1986 Amendment Regulations (SI 2012/3039). All efforts were taken to maximize animal welfare conditions and to reduce the number of animals used in accordance with the European Communities Council Directive of September 20, 2010 (2010/63/EU).

2.2 | Mouse cortical astrocyte cultures

Mixed glial cell cultures were prepared from cerebral cortical tissue from postnatal day one (P1) male and female wild-type C57BL/6 mice (RRID: IMSR_JAX:000664) bred in the BioResources Units of Trinity

College Dublin and the University of Brighton. Two mouse cortices were used per T75 flask preparation. Mixed glial cells were cultured at 37°C and 5% CO₂ in a humidified incubator for 14 days in Dulbecco's modified Eagle's medium/F12 (DMEM/F12; Hyclone SH30023) supplemented with 10% foetal bovine serum (FBS; Labtech, FB-1090) and 1% penicillin/streptomycin (Sigma, P4333), as previously described (Healy et al., 2013; O'Sullivan, Velasco-Estevez, & Dev, 2017). After 14 days in vitro (DIV), T75 flasks containing confluent glial cell cultures were shaken for 2 hr at 200 rpm using an orbital shaker (VWR, Microplate shaker Model No. 980131UK) to eliminate most of the microglia and oligodendrocytes from the glial monolayer. The remaining enriched astrocyte culture was exposed to 0.5% trypsin for 5 min to cause detachment of the glial monolayer and cells were then re-plated in a new T75 flask to further purify the astrocyte culture and eliminate loosely attached microglia. Once the re-plated cells were 80% confluent, they were again exposed to 0.5% trypsin, detached and re-plated in different cell culture substrates for the various experiments described below. Using this method, enriched astrocyte cultures are >95% pure, as previously described (Healy et al., 2013).

2.3 | Immunocytochemistry

After each pharmacological treatment, cells were fixed in 10% formalin solution (Sigma, F1635) for 5 min on ice. Cells were blocked for 18 hr at 4°C in blocking solution containing 1% bovine serum albumin (BSA; Santa-Cruz, sc-2323) and 0.1% Triton X-100 (Sigma, T8787). Primary antibodies were diluted in blocking solution and incubated for 18 hr at 4°C. Cells were washed with PBS containing 0.1% Triton X-100 followed by incubation with secondary antibodies diluted in blocking solution at 22°C for 1 hr in the dark. After several washes, coverslips were mounted on a microscope slide (Clarity, C361) with antifade reagent (ThermoFisher, S36936). Primary antibodies used were: Piezo1 (Abcam, ab128245; RRID: AB_11143245; rabbit polyclonal, dilution 1/500) and GFAP (Abcam, ab4674; RRID: AB_304558; chicken polyclonal, dilution 1/1,000). Secondary antibodies used were biotinylated anti-rabbit (ThermoFisher, A24535; RRID: AB_2536003; dilution 1/1,000), avidin Alexa[®] 488 conjugate (ThermoFisher, A21370; dilution 1/1,000) and Alexa[®] 633 anti-chicken (Alexa, A21103; RRID: AB_2535756; dilution 1/1,000). Imaging was performed using a Leica TCS SP8 confocal microscope.

2.4 | Quantitative reverse transcription PCR (RT-qPCR)

RNA extraction was performed using the RNeasy mini kit (QIAGEN, #74104), following the manufacturer's instructions. The quantity and quality of mRNA was measured by spectrophotometric analysis using a nanodrop (ThermoFisher, NanoDrop[™] One/One^c microvolume). RNA concentration was quantified using the optical density (OD) at 260 nm. The 260/280 nm ratios were used as a measure of quality and only samples with values between 1.8 and 2.0 were considered acceptable. Reverse transcription of the mRNA was performed using the QuantiNova Reverse Transcription Kit (QIAGEN, #205411) in a

³Prime thermocycler (TECHNE, 3PRIMEG/02, serial no. *32288*). The PCR master mix was obtained by mixing SYBR green dye (QIAGEN, #1054596), Quantitect[®] Primer of mouse Piezo1 (Mm_Piezo1_3_SG; QT01199142) or β -actin (Mm_Actb_1_SG; QT00095242) and the cDNA template. The reaction was performed in a Rotor-Gene Q 5plex (QIAGEN, #90158) with PCR cycles of denaturation at 95°C for 5 s and annealing/extension at 60°C for 10 s, 40 times. Data are presented as fold change from control levels after being normalized against β -actin.

2.5 | Western blot

Mouse astrocyte protein samples were obtained by scraping the cell monolayer in RIPA buffer. Samples were run in a 6% SDS-PAGE electrophoresis gel and transferred to PVDF membranes (Millipore, IPVH00010) by wet transfer (buffer composition: 2.5 mM Tris, 19.2 mM Glycine and 5% methanol, pH 8.3) at constant 70 V for 3 hr on ice. Membranes were then blocked in PBS containing 5% BSA and 0.05% Tween-20 for 2 hr at 22°C and incubated with primary antibodies that recognise Piezo1 (Abcam, ab128245; RRID: AB_11143245; dilution 1/300 in blocking buffer) or α -actin (Abcam, ab3280; RRID: AB_303668; dilution 1/2,000 in blocking buffer) for 18 hr at 4°C. After several PBS and PBS-Tween 0.05% washes, membranes were incubated with a goat anti-rabbit HRP-conjugated secondary antibody (GE Healthcare, NA934; RRID: AB_772206; dilution 1/5,000 in blocking buffer) or goat anti-mouse secondary antibody (Sigma, A8924; RRID: AB_258426; dilution 1/5,000 in blocking buffer) for 2 hr at 22°C. Several washes were then performed and PVDF membranes were developed using a chemiluminescent HRP substrate (Millipore, WBKLS0500).

2.6 | MTT assay

Astrocytes were seeded in 96-well plates (Corning) at a density of 15,000 cells/well and grown for 48 hr in DMEM/F12 medium containing 10% FBS. They were then serum-starved for 3 hr prior to stimulation with LPS (100 ng/ml) alone or in combination with GsMTx4 (500 nM) or Yoda1 (10 μ M) for 48 hr. Following each treatment, the cell culture medium was removed and stored for ELISA assays and replaced with 100 μ l of fresh medium supplemented with 1 mg/mL 3-(4,5-dimethylthiazol-2-yl)-2,5-diphenyltetrazolium bromide (MTT) (Invitrogen, M6494) for 3 hr at 37°C. Next, 75 μ l of culture medium was removed and 50 μ l of dimethyl sulfoxide (DMSO) was added. Astrocytes were incubated for 10 min at 37°C and the absorbance in each well was read at a wavelength of 540 nm.

2.7 | JC-1 assay

Changes in mitochondrial potential were measured using a commercially available JC-1 assay kit (Abcam, ab113850) following the manufacturer's instructions. Briefly, astrocytes were seeded in a 96-well plate at a density of 15,000 cells/well and treated as described above for the MTT assay. Thirty minutes prior to the end of each treatment, 10 μ M JC-1 dye was added to each well at a final concentration of



5 μM . After 30 min, the wells were washed twice with dilution buffer. The excitation wavelength was set at 535 ± 17.5 nm and the emission at 590 ± 17.5 nm. Aggregate emission was measured in a BioTek synergy HT microplate reader (BioTek, VT).

2.8 | ELISA assay

Cytokine and chemokine release from astrocytes were quantified using commercially available duo-set ELISA kits (R&D Systems) for mouse IL-6 (DY406), TNF α (DY410), IL-1 β /IL-1F2 (DY401), and CX $_3$ CL1 (DY472). Briefly, 96 well MicroWell™ MaxiSorp™ flat bottom plates (Sigma, 442404) were coated with the capture antibody diluted in PBS for 18 hr at 4°C. Plates were then washed in 0.5% Tween-20 in PBS and blocked with the appropriate reagent diluent for 1 hr at 22°C. The blocking buffer was then removed and the astrocyte culture medium and recombinant protein standards were diluted, added to the wells and incubated for 2 hr at 22°C. The wells were then washed and the detection antibody was added for 2 hr at 22°C. The detection antibody was then washed off and a solution containing streptavidin-HRP secondary antibody was added for 20 min and kept in the dark. The secondary antibody solution was washed off and the substrate solution was added (DY999, R&D Systems) and incubated for 20 min. The reaction was stopped by adding 2 N H $_2$ SO $_4$ to the plate and absorbance was immediately read at 450 nm with wavelength correction at 570 nm.

2.9 | Cell migration assay

A 500 μm wide strip of silicone (silicone sheet of 0.0005" NRV G/G 12" \times 12", SM11074036) was placed down the middle of each well of a 12 well-plate. Astrocytes were then seeded onto each well and grown in supplemented DMEM/F12 media until 90% confluent. Cells were then serum-starved and treated with 100 ng/ml LPS (Sigma, L4391) with or without 10 μM Yoda1 (Tocris, #5586) or 500 nM GsMTx4 (Alomone, STG-100) for 24 hr. The silicone strip was then carefully removed and the 500 μm "wound area" was imaged at "time zero" using a Nikon Eclipse Ti-U microscope with $\times 10$ magnification objective and a Nikon digital sight camera connected to the NIS-Elements BR 3.2 software package (Nikon, Japan). The wound area was imaged again 48 hr post-silicone removal and the change in the width of the area containing no cells was calculated using ImageJ software (<http://imagej.nih.gov/ij>).

2.10 | Live-cell calcium imaging

Astrocytes were seeded onto 25 mm tissue culture plastic coverslips (Sarstedt, #83.1840) in a six well-plate and grown for 72 hr in supplemented DMEM/F12 until 70% confluent. Cells were then serum-starved for 3 hr prior to treatment with or without 100 ng/ml LPS for 24 hr. After treatment, cells were incubated with 3 μM Cal-520AM dye (Abcam, ab171868) in Hank's balanced salt solution (HBSS; no phenol red) supplemented with 10 mM glucose and 25 mM HEPES for 90 min at 37°C, followed by 30 min at 22°C. Cells were protected from bright light at all times. Coverslips were then placed into the Attofluor™ acquisition chamber (Invitrogen) with supplemented HBSS

or HBSS minus Ca $^{2+}$ and Mg $^{2+}$ (HBSS $^{-/-}$). Time-lapse Ca $^{2+}$ imaging was performed at a rate of 0.77 frames per second. Following a 30 s baseline, cells were stimulated with either HBSS or 10 μM Yoda1 for 240 s and stimulated further with 50 μM ATP for 180 s. Extracellular Ca $^{2+}$ imaging experiments were performed with standard HBSS and intracellular Ca $^{2+}$ imaging experiments were performed with HBSS minus Ca $^{2+}$ and Mg $^{2+}$ (HBSS $^{-/-}$). Images were acquired using a Leica SP5 confocal microscope and a $\times 20$ magnification objective.

2.11 | Calcium imaging analysis

Time-lapse Ca $^{2+}$ imaging experiments were saved as Leica.tif files and exported as individual RAW 8 bit.tif images (349 in total per experiment). The maximum intensity projection image was used to create a binary mask allowing for segmentation of the monolayer of astrocytes into individual cells. Image analysis was performed using the R programming environment and EBImage package (Pau, Fuchs, Sklyar, Boutros, & Huber, 2010). Two image segmentation steps were performed. The first identified individual astrocyte nuclei and the second was performed to segment the cytosol of each astrocyte from one another. Nuclear and cytosolic Ca $^{2+}$ responses for each astrocyte were analyzed separately, but both provided very similar results and so only the cytosolic Ca $^{2+}$ imaging quantification is presented here. Absolute changes in cytosolic Ca $^{2+}$ fluorescence intensities were measured for each cell over a 7 min 30 s time period and were then normalized to the baseline fluorescence intensity values for each cell [$\Delta F/F_0$], where F_0 is the average fluorescence intensity of frames 5–15. This converted the absolute changes in cytosolic Ca $^{2+}$ fluorescence intensity to relative changes in Ca $^{2+}$ fluorescence per cell. There were four treatment groups per experiment (a) Control/HBSS, (b) Control/Yoda, (c) LPS/HBSS, and (d) LPS/Yoda. Experiments were conducted either in the presence (Extracellular Ca $^{2+}$) or absence (Intracellular Ca $^{2+}$) of extracellular Ca $^{2+}$ and Mg $^{2+}$ using either Control or LPS pretreated astrocytes. Extracellular Ca $^{2+}$ experiments were repeated $n = 8$ with 3 technical replicates per treatment group, that is, the Ca $^{2+}$ imaging experiments were repeated on 8 separate days using astrocyte cultures from 8 different mouse litters and 3×25 mm coverslips of cells were imaged per group during each live-cell imaging session. Intracellular Ca $^{2+}$ experiments were repeated $n = 6$ with 3 technical replicates per group. In total, the number of astrocytes analyzed per treatment group were as follows: For Extracellular Ca $^{2+}$ experiments, (a) Control/HBSS = 4,286, (b) Control/Yoda = 4,023, (c) LPS/HBSS = 3,980, and (d) LPS/Yoda = 3,915. For Intracellular Ca $^{2+}$ experiments, (a) Control/HBSS $^{-/-}$ = 3,866, (b) Control/Yoda $^{-/-}$ = 3,967, (c) LPS/HBSS $^{-/-}$ = 3,069, and (d) LPS/Yoda $^{-/-}$ = 3,290. In Figures 3 and 5, the relative changes in cytosolic Ca $^{2+}$ fluorescence are expressed as the median value \pm interquartile range (IQR). Moreover, the first 2 min (early) and the last 2 min (late) of HBSS or Yoda1 perfusion are also displayed in Figures 3a and 5a as the mean change in cytosolic Ca $^{2+}$ fluorescence \pm the standard error of the mean.

2.12 | Statistical analysis

All statistical analysis was performed using GraphPad Prism 7 (GraphPad Prism®, RRID:SCR_002798). Assessment of the normality of

data was carried out using the column statistics function and D'Agostino criteria before any further statistical test was performed. When only two groups were compared, a paired Student *t*-test was performed. In cases when three or more groups needed to be compared, repeated measures one-way or two-way ANOVAs were performed and *posthoc* tests were applied with *p* value adjustments using Bonferroni or Holm–Sidak methods. The analysis of proportions was carried out using chi-squared (χ^2) tests in conjunction with the Bonferroni correction for multiple comparisons. *p* values <.05 were considered statistically significant. Further details of the statistical analyses performed are given in each figure legend and Section 3.

3 | RESULTS

3.1 | LPS induces Piezo1 expression in cortical astrocytes

We have recently shown in a rat model of Alzheimer's disease (TgF344-AD) that hippocampal and cortical astrocytes surrounding amyloid plaques upregulate Piezo1 expression. Interestingly, astrocytic Piezo1 expression is enhanced in rats harboring a chronic urinary tract infection with *E. coli* (Velasco-Estevéz et al., 2018). Here, we show that mouse cortical astrocytes exposed to lipopolysaccharide

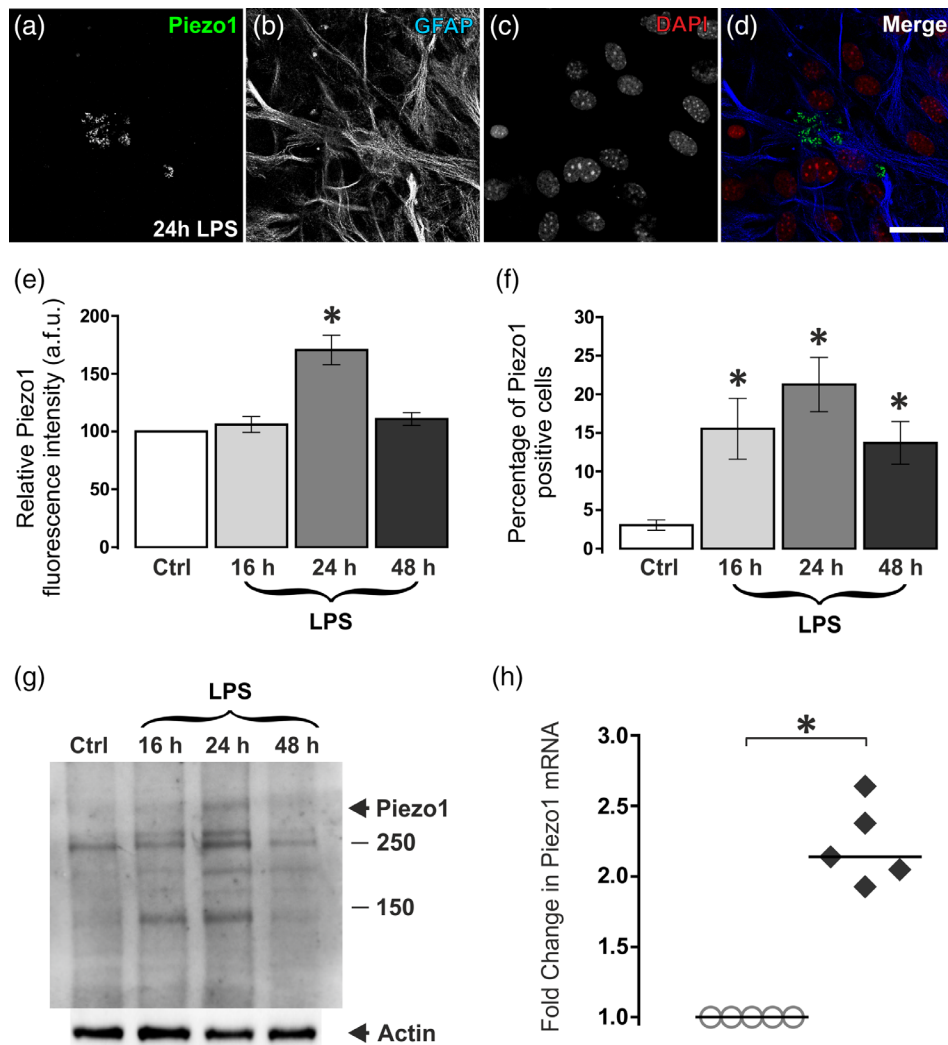


FIGURE 1 Lipopolysaccharide induces Piezo1 expression in astrocytes. Mouse cortical astrocytes were treated with 100 ng/ml LPS for 16, 24, or 48 hr and then immunofluorescently labeled for (a) Piezo1 channels, (b) the astrocytic marker GFAP, and (c) nuclei were counterstained with DAPI. (d) Image represents the above three channels merged. Scale bar = 20 μ m. (e) LPS caused an upregulation of Piezo1 in astrocytes after 24 hr, measured as an increase in Piezo1 fluorescence intensity co-localized with GFAP. (f) Only 2–3% of astrocytes expressed detectable levels of Piezo1 in control nontreated cultures. However, this rose to ~15% after 16 hr LPS and peaked at 20–25% of Piezo1-positive astrocytes following 24 hr LPS exposure. Immunofluorescence experiments were repeated *n* = 5 with two technical replicates per experiment. Results are displayed as mean \pm SEM and were analyzed using a one-way ANOVA with Holm–Sidak *posthoc* test, * *p* < .05. (g) Results obtained through immunofluorescence were confirmed by Western blot (*n* = 3) where a detectable increase in Piezo1 protein (~286 kDa band) was observed in astrocytes after 24 hr LPS exposure. (h) Upregulation of astrocytic Piezo1 24 hr post-LPS exposure was further confirmed by PCR analysis of mRNA transcript levels. PCR experiments were repeated *n* = 5 with two technical replicates per experiment. Results are displayed as fold change from control levels and were analyzed using a paired Student's *t*-test, * *p* < .05 [Color figure can be viewed at wileyonlinelibrary.com]

(LPS) upregulate Piezo1 channel expression. The Gram-negative bacterial endotoxin LPS induces a strong immune reaction in animals and is an agonist of toll-like receptor 4 (TLR4) which is expressed by mouse astrocytes (Nakano et al., 2015). Treatment with 100 ng/ml LPS-induced an inflammatory phenotype in primary cortical astrocytes (Figure 1a–d) and caused an upregulation of Piezo1 channels after 24 hr (Figure 1e). Approximately 2–3% of astrocytes expressed low levels of Piezo1 under noninflammatory conditions and this rose to 20–25% of astrocytes after 24 hr LPS exposure (Figure 1f). Interestingly, Piezo1 expression (measured as immunofluorescence intensity) decreased again after 48 hr exposure to LPS (Figure 1e), but the

proportion of cells expressing low levels of Piezo1 remained above control (Figure 1f). Piezo1 upregulation in astrocytes following 24 hr exposure to LPS was confirmed by Western blot (Figure 1g) and by PCR analysis of mRNA transcript levels (Figure 1h).

3.2 | Piezo1 activation enhances calcium influx in LPS-stimulated astrocytes

Piezo1 is a Ca^{2+} permeable cation channel and since LPS caused an increase in Piezo1 expression in astrocytes (Figure 1), we next investigated the effects of Piezo1 activation on Ca^{2+} influx and Ca^{2+} oscillations in cortical astrocytes. Astrocyte cultures were pretreated either with or without LPS (100 ng/ml) for 24 hr and then loaded with Cal-520AM calcium dye (Figure 2a). Time-lapse Ca^{2+} imaging was performed at a rate of 0.77 frames per second. After a 30 s baseline recording (23 frames), the Piezo1 agonist, Yoda1 (10 μM), was perfused onto nontreated astrocyte cultures (i.e., Control/Yoda) causing an increase in cytosolic Ca^{2+} concentration in 48% of astrocytes (i.e., 52% of cells did not respond to Yoda1). Because Piezo1 channels can be activated by shear stress, HBSS was used to control for extracellular solution perfusion (i.e., Control/HBSS). Here, 46% of cells responded to the addition of HBSS alone (i.e., showed one or more Ca^{2+} peaks) but the increases in cytosolic Ca^{2+} were significantly lower than for Yoda1 (Figure 2b). Similarly, 45% of cells in the LPS-stimulated astrocyte cultures responded to HBSS perfusion, whereas 60% of cells responded to Yoda1 (χ^2 test, $p < .001$) which caused

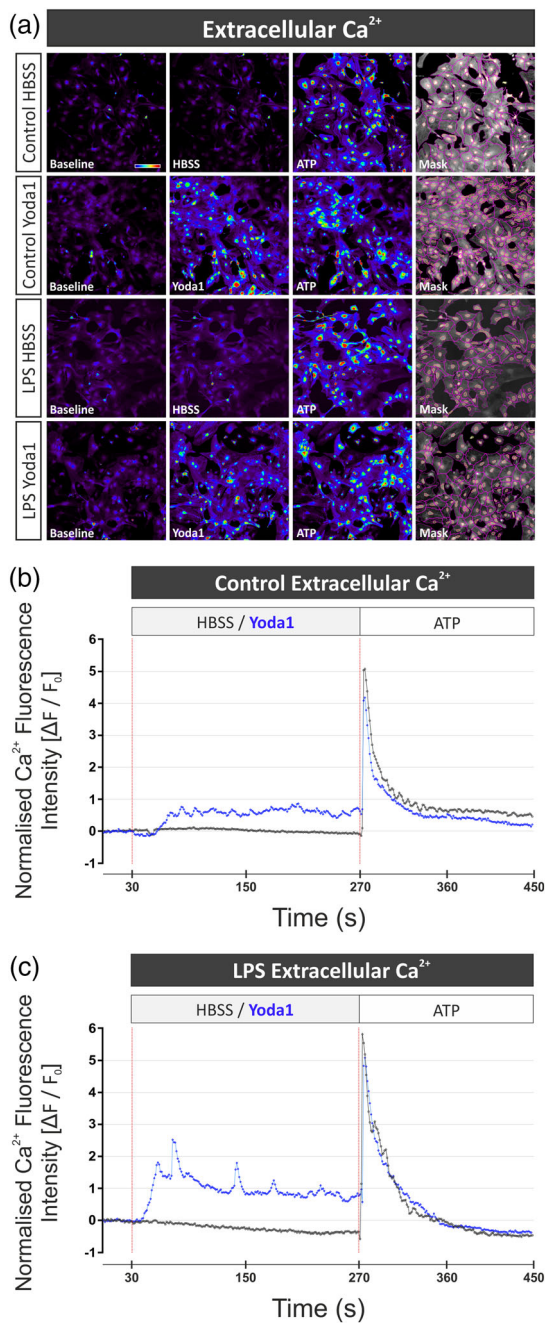


FIGURE 2 Activation of Piezo1 increases intracellular calcium in LPS-reactive astrocytes. Astrocytes were pretreated with or without LPS (100 ng/ml) for 24 hr and loaded with Cal-520AM calcium indicator for 2 hr in Hank's balanced salt solution (HBSS) containing calcium (Ca^{2+}) and magnesium (Mg^{2+}). Immediately prior to Ca^{2+} imaging experiments, astrocytes were transferred to fresh HBSS with Ca^{2+} and Mg^{2+} (i.e., extracellular Ca^{2+} group). (a) Representative confocal images ($\times 20$ magnification) of baseline Ca^{2+} levels and Ca^{2+} influx in response to HBSS, Yoda1 and ATP in control and reactive astrocytes pretreated with LPS for 24 hr. The rainbow-colored palette represents intracellular Ca^{2+} concentrations with dark purple/black signifying low levels of Ca^{2+} and yellow/red representing high levels of Ca^{2+} . Scale bar = 100 μm . The maximum intensity projections of all 349 images were used to segment astrocytes and delineate the nuclear and cytosolic compartments of each individual cell. All data are presented as changes in cytosolic Ca^{2+} influx as opposed to changes in nuclear Ca^{2+} concentrations. Time-lapse Ca^{2+} imaging experiments were performed at a rate of 0.77 frames per second over a 7 min 30 s period (i.e., 349 images in total), which included 30 s baseline, 4 min exposure to 10 μM Yoda1 or fresh HBSS, followed by stimulation with 50 μM ATP for 3 min. (b) Representative traces showing changes in cytosolic Ca^{2+} levels in control and (c) LPS-stimulated astrocytes in response to HBSS (black) and Yoda1 (blue). There was a 30 s baseline, at which point HBSS or Yoda1 was perfused onto astrocyte cultures for 4 min followed by ATP stimulation (at 270 s) for a further 3 min. Yoda1 caused larger elevations in cytosolic Ca^{2+} in LPS-treated astrocytes compared to control nonreactive astrocytes [Color figure can be viewed at wileyonlinelibrary.com]

much larger Ca^{2+} influxes (Figure 2c). This was presumably due to the upregulation of Piezo1 channels in LPS-stimulated astrocytes (Figure 1).

The median area under the curve (AUC with arbitrary fluorescence units; a.f.u.) was negative in response to HBSS, that is, -5.2 a.f.u. (-36.9 , $+41.4$ IQR) suggesting a small net efflux of intracellular Ca^{2+} (Figure 3a). Yoda1, on the other hand, induced an increase in Ca^{2+} influx, with the median AUC measured as $+48.3$ a.f.u. (-3.2 , $+158.1$ IQR). Interestingly, for control astrocytes perfused with HBSS or Yoda1 and for LPS-stimulated cultures perfused with HBSS, 9–10% of cells responded with two or more Ca^{2+} peaks (Figure 3b) over the 4 min time-frame. In contrast, astrocytes pretreated with LPS and

perfused with Yoda1 displayed a doubling (20%) in the proportion of cells that responded with two or more Ca^{2+} peaks (χ^2 test, $p < .001$), suggesting that Piezo1 increases Ca^{2+} oscillations in LPS-reactive astrocytes (Figure 3b).

3.3 | Activation of Piezo1 in LPS-stimulated astrocytes modifies their response to ATP

After recording control and LPS-stimulated astrocyte Ca^{2+} responses to both HBSS and Yoda1 for 4 min, all four groups of cells were then perfused with $50 \mu\text{M}$ ATP. Time-lapse images were captured for a further 3 min (140 frames) to determine the proportions of astrocytes

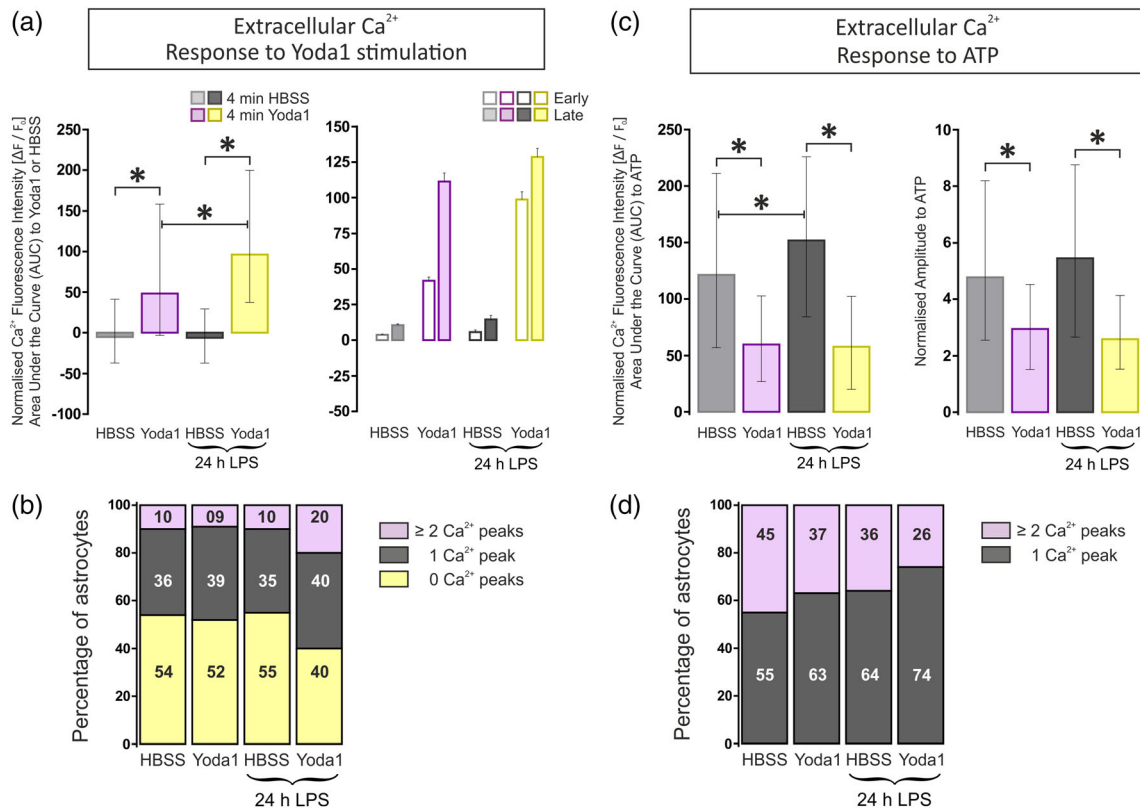


FIGURE 3 Activation of Piezo1 increases calcium oscillations in LPS-stimulated astrocytes. (a) HBSS was used as a control for extracellular medium perfusion because Piezo1 channels are mechanosensitive and can be activated by shear stress. However, HBSS did not induce any appreciable increase in Ca^{2+} influx into control or LPS-stimulated astrocytes. Yoda1, on the contrary, caused an increase in Ca^{2+} influx into control astrocytes and a significantly larger influx of Ca^{2+} into LPS-stimulated astrocytes ($+48.3$ [-3.2 , $+158.1$ IQR] vs. $+96.3$ [37.5 , 200.0 IQR] arbitrary fluorescence units; a.f.u.). Data are presented as median \pm interquartile range and were analyzed using a two-way ANOVA with Bonferroni posthoc test, $*p < .05$. The first 2 min of HBSS/Yoda1 exposure (designated “early”) was also analyzed separately to the last 2 min (“late”). In general, there was more Ca^{2+} influx in the latter 2 min period than the first 2 min, both in control and LPS-treated astrocytes, suggesting a delayed and prolonged increase in cellular Ca^{2+} levels in response to Yoda1 and, hence, Piezo1 channel activation. Early- and late-phase Yoda1 exposure data are presented as mean \pm the standard error of the mean (SEM). (b) Approximately 9–10% of control astrocytes stimulated with either HBSS or Yoda1, and LPS-stimulated astrocytes perfused with HBSS, displayed 2 or more Ca^{2+} peaks (i.e., Ca^{2+} oscillations). Interestingly, LPS-treated astrocytes stimulated with Yoda1 displayed double the number of cells expressing Ca^{2+} oscillations (i.e., 20%), χ^2 test, $p < .001$. This suggests that upregulation of Piezo1 in LPS-treated astrocytes may promote oscillatory Ca^{2+} activity in response to mechanical stimuli. (c) However, Yoda1-stimulated astrocytes responded less to ATP perfusion compared to HBSS-stimulated cells. Both the amplitude and the area under the curve (AUC) of the Ca^{2+} response to ATP was significantly reduced in Yoda1-stimulated astrocytes. Data are presented as median \pm interquartile range and were analyzed using a two-way ANOVA with Bonferroni posthoc test, $*p < .05$. Astrocytes pretreated with LPS for 24 hr showed the largest AUC and peak amplitude to ATP, suggesting reactive astrocytes are more responsive to purinergic receptor stimulation. (d) However, only 26% of reactive astrocytes stimulated with Yoda1 displayed Ca^{2+} oscillations to ATP, whereas 36–45% of cells in the other three groups displayed ATP-induced Ca^{2+} oscillations. Therefore, Yoda1-mediated activation of Piezo1 appeared to dampen ATP-induced Ca^{2+} oscillations in astrocytes, χ^2 test, $p < .001$ [Color figure can be viewed at wileyonlinelibrary.com]

that display ATP-induced Ca^{2+} oscillations. Control and LPS-stimulated astrocytes preperfused with HBSS displayed ATP-induced Ca^{2+} peaks that were larger in amplitude to those elicited by astrocytes preperfused with Yoda1 (Figure 3c). This is because the Control/HBSS and LPS/HBSS groups displayed negative median AUC Ca^{2+} responses to HBSS perfusion and, therefore, had low basal Ca^{2+} levels upon the addition of ATP. This enabled them to respond with large ATP-induced Ca^{2+} peaks. The LPS/HBSS group showed the largest AUC Ca^{2+} response to ATP perfusion, that is, +151.9 a.f.u (+84.2, +225.5 IQR). Interestingly, astrocytes that displayed the highest number of Ca^{2+} oscillations to Yoda1 (i.e., the LPS/Yoda1 group) responded with the lowest number of Ca^{2+} peaks following ATP

perfusion, that is, 26% of astrocytes in the LPS/Yoda1 group displayed 2 or more Ca^{2+} peaks whereas 45% of the Control/HBSS group showed ATP-induced Ca^{2+} oscillations (χ^2 test, $p < .001$; Figure 3d). Taken together, our data indicate that Yoda1 enhances Ca^{2+} oscillations in LPS-stimulated astrocytes (due to upregulation of Piezo1), but this increases basal Ca^{2+} levels and consequently reduces the proportion of cells that display Ca^{2+} oscillations in response to ATP.

3.4 | Piezo1 activation enhances calcium release from intracellular stores in LPS-stimulated astrocytes

To determine the effects of Piezo1 activation on Ca^{2+} release from internal stores, extracellular Ca^{2+} and magnesium (Mg^{2+}) were removed from the medium, that is, HBSS minus Ca^{2+} and Mg^{2+} ($\text{HBSS}^{-/-}$). Experiments were repeated, as above, with the same four groups of astrocytes, that is, Control/ $\text{HBSS}^{-/-}$, Control/ $\text{Yoda1}^{-/-}$, LPS/ $\text{HBSS}^{-/-}$, and LPS/ $\text{Yoda1}^{-/-}$ (Figure 4a–c). Interestingly, $\text{Yoda1}^{-/-}$ (dissolved in HBSS minus Ca^{2+} and Mg^{2+}) caused a large efflux of Ca^{2+} from control astrocytes; -63.8 a.f.u ($-98.6, -7.3$ IQR), but LPS-stimulated astrocytes showed a net increase in cytosolic Ca^{2+} levels; $+11.0$ a.f.u ($-50.6, +75.8$ IQR) (Figure 5a). As such, Yoda1 increased the proportion of cells in nontreated astrocytes that displayed zero positive peak deflections in intracellular Ca^{2+} (i.e., Control/ $\text{Yoda1}^{-/-}$ 55% vs 34% Control/ $\text{HBSS}^{-/-}$, χ^2 test, $p < .001$). This was due to the large net efflux of Ca^{2+} to the extracellular medium and, therefore, the decrease in basal Ca^{2+} levels in the Control/ $\text{Yoda1}^{-/-}$ group. However, comparable proportions of cells (24%) in the Control/ $\text{Yoda1}^{-/-}$ group responded with one positive Ca^{2+} peak compared to astrocytes in the Control/ $\text{HBSS}^{-/-}$ group (27%). Therefore, the difference lay in the proportion of cells that displayed Ca^{2+} oscillations (i.e., 2 or more peaks). Twenty one percent of Control/ $\text{Yoda1}^{-/-}$ cells displayed Ca^{2+} oscillations in response to Yoda1 whereas 39% of cells in the

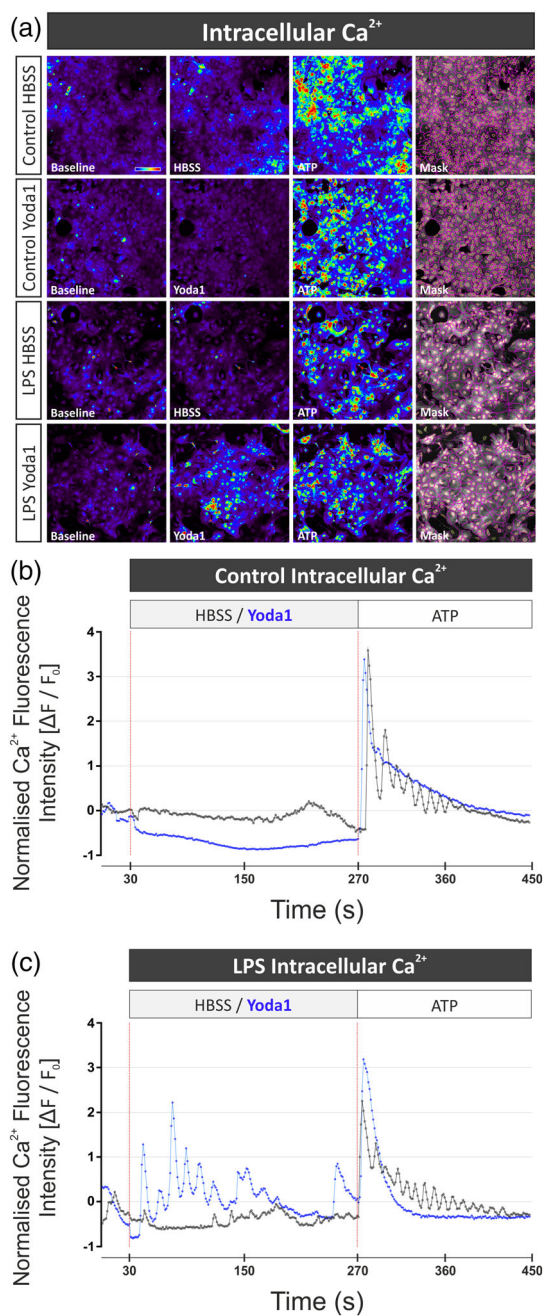


FIGURE 4 Activation of Piezo1 increases calcium release from intracellular stores in LPS-reactive astrocytes. Time-lapse Ca^{2+} imaging experiments were repeated in astrocyte cultures in the absence of extracellular calcium and magnesium (i.e., $\text{HBSS}^{-/-}$ minus Ca^{2+} and Mg^{2+}) in order to assess intracellular store-driven Ca^{2+} fluxes regulated by Piezo1 channels. Astrocytes were pretreated with or without LPS (100 ng/ml) for 24 hr and loaded with Cal-520AM calcium indicator for 2 hr in Hank's balanced salt solution (HBSS) containing calcium (Ca^{2+}) and magnesium (Mg^{2+}). Immediately prior to Ca^{2+} imaging experiments, astrocytes were transferred to fresh $\text{HBSS}^{-/-}$ without Ca^{2+} and Mg^{2+} (i.e., intracellular Ca^{2+} group). (a) Representative confocal fluorescence images of astrocytes loaded with Cal-520AM dye and stimulated with $\text{HBSS}^{-/-}$, $\text{Yoda1}^{-/-}$, and $\text{ATP}^{-/-}$. The rainbow-colored palette describes low versus high levels of intracellular Ca^{2+} concentrations. Scale bar = 100 μm . (b) Representative traces of control and (c) LPS-treated astrocytes stimulated with $\text{HBSS}^{-/-}$ or $\text{Yoda1}^{-/-}$ and $\text{ATP}^{-/-}$ in the absence of extracellular Ca^{2+} and Mg^{2+} . Yoda1 caused a decrease in intracellular Ca^{2+} levels in control astrocytes, possibly through depletion of intracellular stores and efflux of Ca^{2+} from the cytosol. However, $\text{Yoda1}^{-/-}$ caused an increase in internal store-mediated Ca^{2+} elevations in LPS-reactive astrocytes [Color figure can be viewed at wileyonlinelibrary.com]

Control/HBSS^{-/-} group showed Ca²⁺ oscillations following HBSS^{-/-} perfusion (Figure 5b). This indicates that Yoda1^{-/-} decreases Ca²⁺ oscillations driven by internal stores in control nonreactive astrocytes (χ^2 test, $p < .001$).

The opposite was true for the LPS/HBSS^{-/-} group, however. A similar proportion of nonresponders (32%) were measured in LPS/HBSS^{-/-} treated astrocytes compared to 34% of cells in the Control/HBSS^{-/-} group. However, there was a 10% increase in cells displaying Ca²⁺ oscillations (LPS/HBSS^{-/-} 49% vs. 39% Control/HBSS^{-/-}, χ^2 test, $p < .001$), suggesting that LPS-stimulated astrocytes are more “responsive” to shear stress and display more internal store-driven Ca²⁺ oscillations. Interestingly, Yoda1 induced a modest 4% increase in the proportion of cells that displayed Ca²⁺ oscillations in LPS-stimulated cultures (LPS/HBSS^{-/-} 49% vs. 53% LPS/Yoda1^{-/-}, χ^2 test, $p = .008$). However, Yoda1 caused a greater increase in the proportion of cells that respond with just one peak in intracellular Ca²⁺ (LPS/HBSS^{-/-} 19% vs. 28% LPS/Yoda1^{-/-}; Figure 5b). This increase in internal store-driven Ca²⁺ oscillations in LPS-

treated astrocytes exposed to Yoda1 impacted their subsequent responses to ATP perfusion. As such, 68% of astrocytes in the LPS/Yoda1^{-/-} group responded to ATP with one positive peak in intracellular Ca²⁺ versus 61% of LPS/HBSS^{-/-} astrocytes (χ^2 test, $p < .001$). However, this meant that 39% of LPS/HBSS^{-/-} astrocytes showed ATP-induced Ca²⁺ oscillations versus 32% of the LPS/Yoda1^{-/-} group. The proportion of cells showing Ca²⁺ oscillations to ATP in the Control/Yoda1^{-/-} group was even lower again (24%) compared to the Control/HBSS^{-/-} group (33%). Therefore, while Yoda1 caused an increase in ATP-induced Ca²⁺ release from intracellular stores in control astrocytes (Figure 5c) and increased the percentage of cells that responded with one Ca²⁺ peak following ATP perfusion (Figure 5d), astrocyte cultures in the Control/Yoda1^{-/-} group displayed the lowest proportion of cells (24%) that oscillated in response to Yoda1 perfusion (Figure 5d). Taken together, LPS-stimulated astrocytes respond to Yoda1 by increasing intracellular Ca²⁺ levels and internal store-driven Ca²⁺ oscillations compared to astrocytes perfused with control HBSS^{-/-}. However, LPS/Yoda1^{-/-}

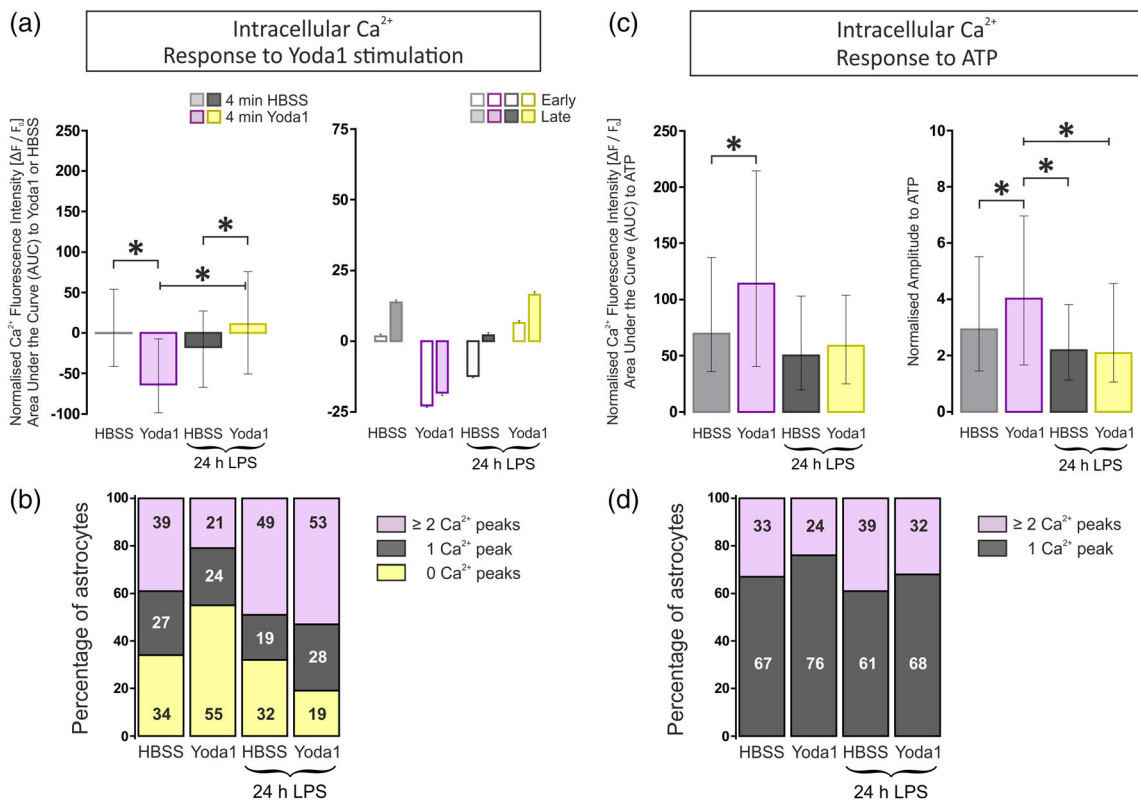


FIGURE 5 Yoda1 decreases ATP-induced calcium oscillations in astrocytes. (a) In control astrocytes, Yoda1 caused an efflux of Ca²⁺ from the cytosol to the extracellular space resulting in a decrease in Cal-520AM fluorescence intensity. In reactive astrocytes pretreated with LPS for 24 h, however, Yoda1 caused increases in cytosolic Ca²⁺ levels, presumably through release from intracellular stores but with a reduced efflux of Ca²⁺ ions to the extracellular space. Data for the total 4 min treatment period are represented as the median ± the interquartile range and were analyzed using a two-way ANOVA with Bonferroni posthoc test, $*p < .05$. The “early” and “late” phase data represent the mean ± SEM. (b) Control astrocytes bathed in HBSS minus Ca²⁺ and Mg²⁺ and stimulated with Yoda1 displayed the lowest proportion of cells responding with multiple Ca²⁺ oscillations (21%). This was due to the large efflux of Ca²⁺ in response to Yoda1. However, reactive astrocytes stimulated with Yoda1 displayed the largest proportion of intracellular store-driven Ca²⁺ oscillations (53%), χ^2 test, $p = .008$. (c) Interestingly, control astrocytes bathed in HBSS minus Ca²⁺ and Mg²⁺ and stimulated with Yoda1 showed the highest Ca²⁺ response to ATP, both in peak amplitude and AUC. This is likely due to the very low levels of cytosolic Ca²⁺ post-Yoda1 stimulation, that is, the relative increases in Ca²⁺ appear very high when the basal levels are low. (d) Moreover, Yoda1 decreased the percentage of control cells that displayed ATP-induced store-driven Ca²⁺ oscillations (24%), χ^2 test, $p < .001$, suggesting that when basal Ca²⁺ levels are low, purinergic receptor stimulation does not induce many store-driven Ca²⁺ oscillations [Color figure can be viewed at wileyonlinelibrary.com]

astrocytes were less responsive to ATP, presumably because their basal Ca^{2+} levels were higher than the Control/Yoda1^{-/-} group.

3.5 | Blocking Piezo1 channels enhances cell migration in LPS-stimulated astrocytes

Astrocytes were treated with LPS (100 ng/ml) for 48 hr in the presence or absence of either Yoda1 (agonist) or GsMTx4 (antagonist) to activate or inhibit Piezo1 channels, respectively. Neither activation nor inhibition of Piezo1 affected cell viability (Figure 6a) or

mitochondrial stress (Figure 6b). Because Piezo1 channels have been shown previously to regulate endothelial (Eisenhoffer et al., 2012), fibroblast (Chubinskiy-Nadezhdin et al., 2019) and cancer cell migration (McHugh, Murdoch, Haslett, & Sethi, 2012), we next investigated if Piezo1 channels modulate astrocyte migration. Control astrocytes were grown to confluency over a 500 μm silicone strip running down the center of a 35 mm cell culture well. The silicone strip was then peeled away to create a reproducible “wound healing” type assay to measure collective astrocyte migration velocities over a 48-hour period. Astrocytes were exposed to either Yoda1 (10 μM) or GsMTx4

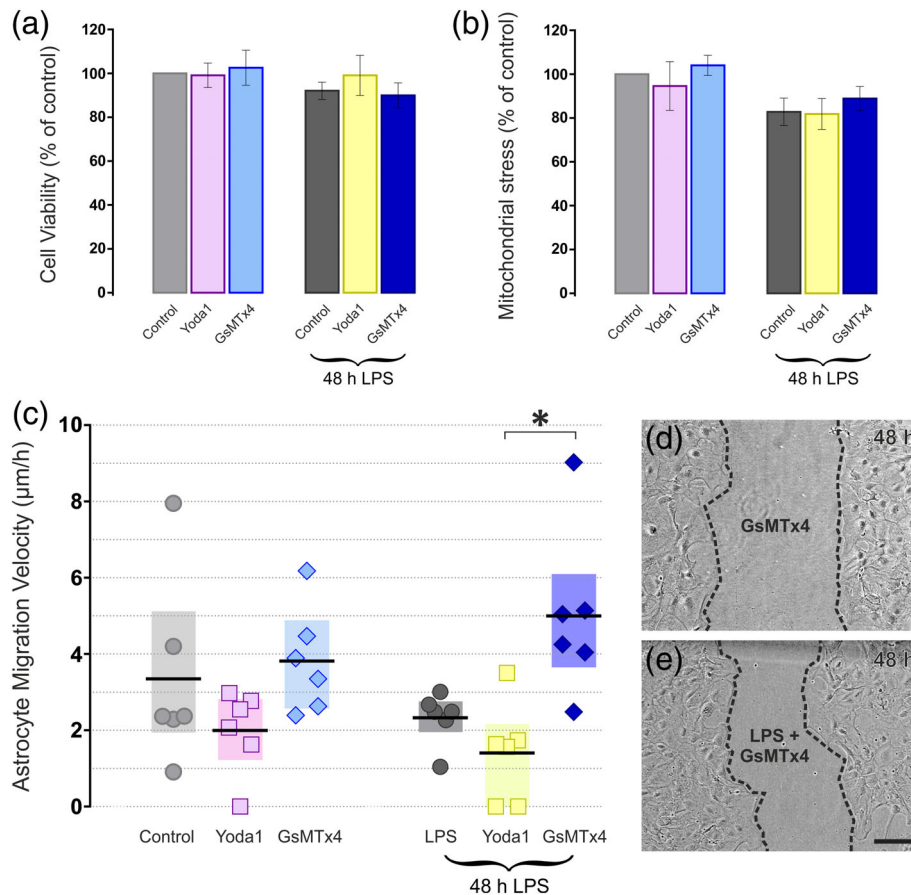


FIGURE 6 Piezo1 channels modulate astrocyte migration (a) Astrocyte cultures were treated with the Piezo1 agonist, Yoda1 (10 μM), or the blocking peptide, GsMTx4 (500 nM), in the presence or absence of LPS (100 ng/mL) for 48 hr. Neither Yoda1 nor GsMTx4 significantly affected cell viability of control or LPS-stimulated astrocytes as measured by the MTT assay. Data are presented as a percentage of the mean control fluorescence intensity (540/590 nm) \pm SEM from $n = 6$ independent experiments. Results were analyzed using a two-way ANOVA with the Holm–Sidak posthoc test. (b) To confirm that Piezo1 activation with Yoda1 had negligible effects on cellular stress, the JC-1 assay was performed to measure changes in the mitochondrial membrane potential of control and LPS-stimulated astrocytes. Neither Yoda1 nor GsMTx4 caused significant mitochondrial stress in LPS-treated astrocyte cultures. Data are presented as the mean absorbance levels (at 570 nm) \pm SEM normalized to control values ($n = 6$ independent experiments). Results were analyzed using a two-way ANOVA with the Holm–Sidak posthoc test. (c) Next, a “wound healing” type cell migration assay was performed to assess changes in the speed of astrocyte migration in response to Piezo1 activation and inhibition. Activation of Piezo1 with Yoda1 did not significantly affect astrocyte migratory velocity in control (2.0 ± 0.4 vs. 3.3 ± 1.0 $\mu\text{m}/\text{hr}$) or LPS-stimulated cultures (1.4 ± 0.5 vs. 2.3 ± 0.3 $\mu\text{m}/\text{hr}$). Similarly, inhibition of Piezo1 with GsMTx4 did not alter astrocyte migration velocity in control (3.8 ± 0.6 vs. 3.3 ± 1.0 $\mu\text{m}/\text{hr}$) or LPS-stimulated cultures (5.0 ± 0.9 vs. 2.3 ± 0.3 $\mu\text{m}/\text{hr}$). However, there were significant differences in the velocities of LPS-stimulated astrocytes exposed to Yoda1 versus GsMTx4 (1.4 ± 0.5 vs. 5.0 ± 0.9 $\mu\text{m}/\text{hr}$), suggesting that Piezo1 channel activation in reactive astrocytes inhibits the speed of collective cell migration. Data are presented as the mean velocity ($\mu\text{m}/\text{hr}$) over a 48-hr period (black horizontal line), the interquartile range (shaded rectangle) and the absolute velocity values of $n = 6$ independent experiments. Differences were analyzed using a two-way ANOVA with the Holm–Sidak post hoc test and $*p < .05$. (d) and (e) are representative images of the migration assay showing (d) control and (e) LPS-stimulated astrocytes after 48 hr treatment with GsMTx4. Scale bar = 100 μm [Color figure can be viewed at wileyonlinelibrary.com]

(500 nM) for 48 hr, neither of which had any significant effect on astrocyte migration compared to nontreated control cells which migrated at an average velocity of $3.3 \pm 1.0 \mu\text{m/hr}$ (Figure 6c). Astrocytes treated with GsMTx4 migrated at $3.8 \pm 0.6 \mu\text{m/hr}$ but this was not statistically significantly faster than astrocytes treated with Yoda1 ($2.0 \pm 0.4 \mu\text{m/hr}$). In order to assess the role of Piezo1 in cell migration, astrocytes were stimulated with LPS to trigger Piezo1 expression and migratory velocities were monitored over 48 hr. LPS-stimulated astrocytes exposed to GsMTx4 for 48 hr migrated at a velocity of $5.0 \pm 0.9 \mu\text{m/hr}$. This was not significantly faster than astrocytes treated with LPS alone ($2.3 \pm 0.3 \mu\text{m/hr}$) but was significantly faster than LPS-stimulated astrocytes exposed to Yoda1 ($1.3 \pm 0.5 \mu\text{m/hr}$; Figure 6c). This suggests that Piezo1 channel activity regulates astrocyte migration under neuroinflammatory conditions (Figure 6d,e).

3.6 | Yoda1 inhibits cytokine and chemokine release from LPS-stimulated astrocytes

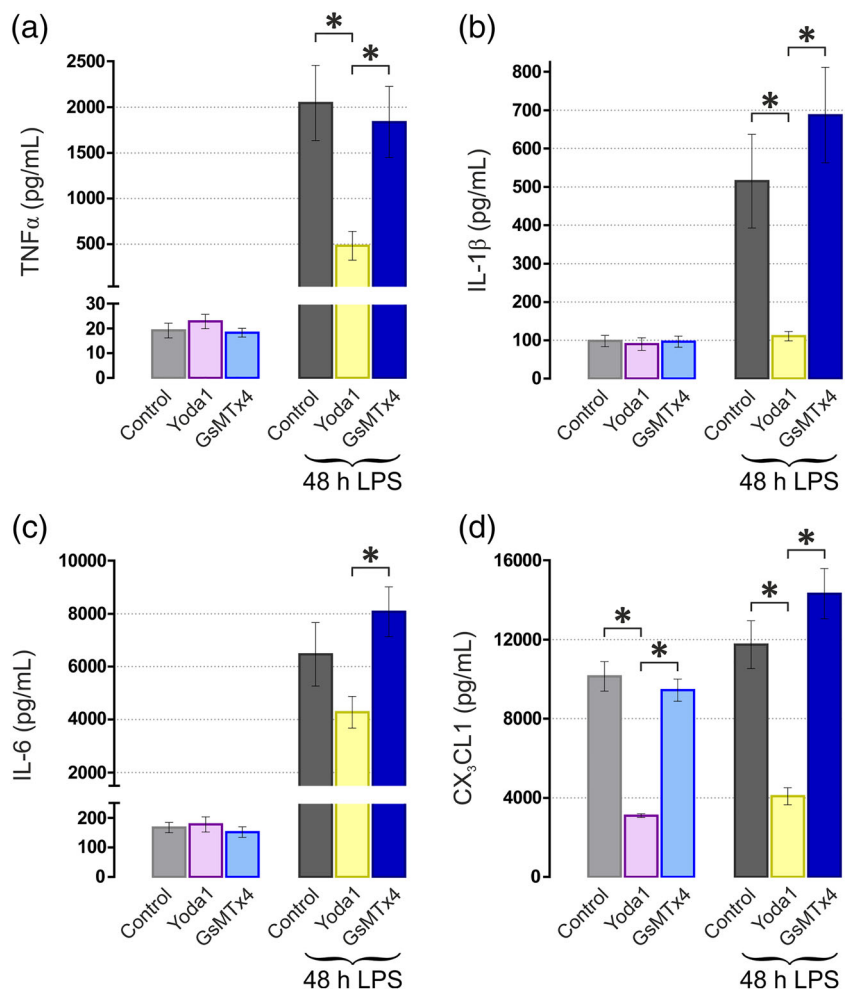
LPS is a well-known trigger of inflammation and cytokine release from astrocytes (Liddelow et al., 2017). Our next aim was to investigate if modulating Piezo1 activity alters proinflammatory cytokine or chemokine release from cortical astrocyte cultures. Treating astrocytes with Yoda1 for 48 hr, in the presence of LPS, decreased the release of TNF α

(484 ± 157 vs. $2,046 \pm 410$ pg/ml; Figure 7a), IL-1 β (111 ± 12 vs. 515 ± 122 pg/ml; Figure 7b), and CX₃CL1 ($4,089 \pm 430$ vs. $11,745 \pm 1,210$ pg/ml; Figure 7d), but had no significant effect on IL-6 release ($4,274 \pm 601$ vs. $6,468 \pm 1,202$ pg/ml; Figure 7c). However, there was a statistically significant difference in the amount of IL-6 released from astrocytes treated with LPS/Yoda1 ($4,274 \pm 601$ pg/mL) versus LPS/GsMTx4 ($8,076 \pm 947$ pg/ml; Figure 7c). Interestingly, Yoda1 also decreased CX₃CL1 release from control astrocytes ($3,105 \pm 94$ vs. $10,140 \pm 741$ pg/ml). Taken together, our results suggest that LPS exposure upregulates Piezo1 in a modest proportion of astrocytes (~25%) and, when activated, Piezo1 channels increase intracellular Ca²⁺ oscillations and inhibit the production and release of pro-inflammatory cytokines and chemokines (Figure 8). Astrocytic Piezo1 may, therefore, act to dampen CNS neuroinflammation.

4 | DISCUSSION

Our understanding of glial cell biology and biophysics has advanced rapidly over the last two decades and it is now widely accepted that astrocytes resident in different brain regions exhibit heterogeneity in morphology and function (Matias, Morgado, & Gomes, 2019). Local sub-populations of astrocytes within a common neuronal ensemble also appear to exhibit distinct functional groupings, such as the A1

FIGURE 7 Piezo1 channels modulate cytokine and chemokine release from astrocytes. (a) Cytokine and chemokine release from control and LPS-stimulated astrocytes were measured after 48 hr of either Yoda1 or GsMTx4 exposure. GsMTx4 peptide (500 nM) had little or no effect on cytokine release from reactive astrocytes. However, LPS-stimulated astrocytes exposed to 10 μM Yoda1 for 48 hr showed a significant decrease in (a) TNF α and (b) IL-1 β release into the cell culture medium, as measured by ELISA. (c) Yoda1 did not cause a significant reduction in IL-6 release from astrocytes when compared to the LPS only group ($4,274 \pm 601$ vs. $6,468 \pm 1,202$ pg/ml), but levels of IL-6 release in the LPS/Yoda1 group were significantly less than the LPS/GsMTx4-treated astrocytes ($8,076 \pm 947$ pg/ml). (d) Yoda1 also caused a significant decrease in CX₃CL1 release from both control ($3,105 \pm 94$ vs. $10,140 \pm 741$ pg/ml) and LPS-stimulated astrocytes ($4,089 \pm 430$ vs. $11,745 \pm 1,210$ pg/ml). Data from the ELISA assays are presented as mean \pm SEM. TNF α , IL-1 β , and IL-6 ELISA's were repeated $n = 5$ and CX₃CL1 ELISA was repeated $n = 3$. Differences were analyzed using a two-way ANOVA with the Holm-Sidak posthoc test and $*p < .05$ [Color figure can be viewed at wileyonlinelibrary.com]



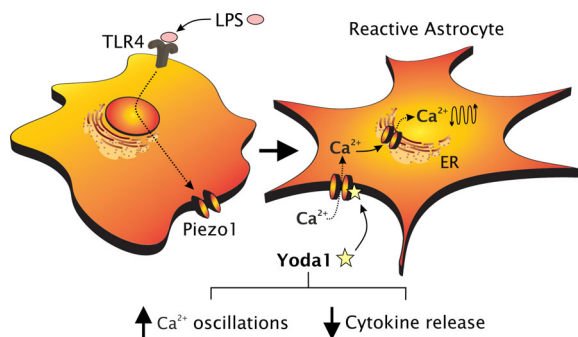


FIGURE 8 Proposed mechanism to explain Piezo1-mediated anti-inflammatory effects in LPS-stimulated astrocytes. Primary cortical astrocytes treated for 24 hr with LPS upregulate Piezo1 expression. Activating Piezo1 channels with Yoda1 causes calcium (Ca^{2+}) influx and increases intracellular store-driven Ca^{2+} oscillations. In addition to its expression at the outer cell membrane, Piezo1 may localize to the ER of reactive astrocytes, thus enhancing intracellular Ca^{2+} release following Yoda1 exposure. Indeed, Syeda et al. (2015) have also reported that chelation of extracellular Ca^{2+} with EGTA did not completely abolish the calcium responses observed in HEK293T cells following Yoda1 stimulation. Alternatively, Yoda1 may also induce nonspecific effects independent of Piezo1. In the absence of extracellular Ca^{2+} , Yoda1 triggered release of Ca^{2+} from intracellular stores in reactive astrocytes (Figure 5a) and increased Ca^{2+} oscillations compared to Yoda1-stimulated control astrocytes (Figure 5b). Yoda1 also decreased IL-1 β , TNF α , and CX $_3$ CL1 release from LPS-stimulated astrocytes, suggesting that Piezo1 may play a role in dampening neuroinflammation in the brain. More work is needed to investigate if there is a link between Piezo1-mediated Ca^{2+} oscillations, reduced ATP-responsiveness and inhibition of pro-inflammatory cytokine release from reactive astrocytes [Color figure can be viewed at wileyonlinelibrary.com]

and A2 phenotypes recently described (Liddelow et al., 2017). Astrocytes sense and react to the local biochemical milieu of the brain parenchyma, as well as to the mechanical properties of the extracellular matrix and neighboring cells, particularly after CNS injury (Bowers, Fiori, Khadela, Janmey, & Galie, 2019; Rocha, Ferraz-Nogueira, Barrias, Relvas, & Pego, 2015). Here, primary mouse astrocyte cultures were used to investigate several potential functions of astroglial Piezo1 channels in the cerebral cortex during a neuroinflammatory stimulus. Our data suggest that the bacterial endotoxin, LPS, triggers Piezo1 expression in cortical astrocytes which normally express very low levels of mechanosensitive Piezo1 ion channels, at least under control conditions in vitro, although we and others have detected astrocytic Piezo1 expression in vivo (Choi, Sun, & Jakobs, 2015; Velasco-Estevéz et al., 2018). However, not all LPS-stimulated astrocytes (~25%) expressed the Piezo1 protein in vitro, suggesting those that did may have slightly different functions to their Piezo1-negative neighbors. Alternatively, astrocytes in culture may display a range of responses to LPS stimulation. For instance, the levels of TLR4 receptor expression may vary between functionally distinct sub-populations of cultured astrocytes (El-Hage, Podhaizer, Sturgill, & Hauser, 2011) which could also explain why only ~25% of astrocytes expressed Piezo1 post-LPS treatment.

4.1 | Astrocyte migration

Astrocyte migration was assessed using a two-dimensional wound healing-type assay and, therefore, resembled an unrestricted collective cell migration. Cell migration can be classified using several criteria, for example, single cell vs collective migration (Rorth, 2009), amoeboid versus integrin-dependant (Friedl & Brocker, 2000) or confined vs unrestricted migration (Hung et al., 2016). In the healthy adult brain, astrocytes do not generally migrate (Zhan et al., 2017). However, in neuroinflammatory states or following traumatic tissue injury, reactive astrocytes can change shape, become hypertrophic (Sofroniew & Vinters, 2010), contribute to glial scarring (Buffo, Rolando, & Ceruti, 2010) and display integrin-dependent migration (Cardenas, Kong, Alvarez, Maldonado, & Leyton, 2014). Interestingly, before its characterisation as a mechanosensitive ion channel, McHugh et al. (2010) described an important role for Piezo1 in maintaining integrin-mediated cell adhesion in epithelial cells. Piezo1 reportedly recruits the small GTPase, R-Ras, to the ER leading to release of calcium from internal stores, activation of calpain signaling, cleavage of talin and enhancement of integrin affinity, thus strengthening cell adhesions. Moreover, knocking down Piezo1 using siRNA increased migration of lung epithelial cells through loss of integrin-mediated cell adhesions (McHugh et al., 2012). Therefore, it has been suggested that Piezo1 expression may influence the metastatic invasiveness of cancer cells (Li et al., 2015; Yang et al., 2014). However, Piezo1 antagonism appears to have different effects on migration in different cell types. Treating human umbilical vein endothelial cells (HUVECs) or prostate cancer cell lines (PC-3 and LNCaP) with GsMTx4 causes a decrease in cell migration (Li et al., 2014; Maroto, Kurosky, & Hamill, 2012) but enhances neurite outgrowth in *Xenopus* spinal cord explants (Jacques-Fricke, Seow, Gottlieb, Sachs, & Gomez, 2006). More recently, Song et al. (2019) have shown that Piezo1 activation can inhibit neural regeneration in *Drosophila*. Here, we show that astrocytes exposed to LPS (to induce Piezo1 expression) and GsMTx4 (to simultaneously block Piezo1 channel opening) migrate faster than astrocytes stimulated with LPS and Yoda1 (which activates Piezo1 channels). It is possible that GsMTx4 modulates integrin affinity in reactive astrocytes, thus enhancing collective cell migration velocity. In agreement with our findings, Chubinskiy-Nadezhdin et al. (2019) have also recently reported that Yoda1 decreases fibroblast migratory speed. Therefore, we hypothesize that activation of Piezo1 may attenuate the reactive phenotype of astrocytes in vivo by dampening their migratory capacity in neuroinflammatory disorders of the ageing brain, for example.

4.2 | Piezo1-mediated Ca^{2+} signaling in astrocytes

Under noninflammatory control conditions, cultured astrocytes appeared largely devoid of Piezo1 expression; although ~48% of cells responded to Yoda1 application with small influxes of calcium (Figure 3a,b). Therefore, Piezo1 channels may be expressed at low levels, which are undetectable with the antibody used here. As a positive modulator of the Piezo1 ion channel, Yoda1 binds directly to

Piezo1 to stabilize the open conformation of the channel pore, thus decreasing the threshold for mechanical activation (Cahalan et al., 2015; Lacroix, Botello-Smith, & Luo, 2018; Syeda et al., 2015). However, Yoda1 may also exert some off-target effects, such as increasing the likelihood that other types of Ca^{2+} -permeable channels will open, as suggested by Dela Paz and Frangos (2018) who showed that Yoda1 activates both Akt and ERK1/2 signaling in endothelial cell types, independent of Piezo1. The authors argue that Yoda1 may activate one or more transient receptor potential (TRP) cation channels, which could explain how Akt and ERK1/2 become phosphorylated. This could also explain why, in our study, ~48% of control astrocytes responded to Yoda1 with small influxes of Ca^{2+} , but we could detect only ~3% of cells that expressed Piezo1 (as quantified by immunofluorescence). Following 24 hr stimulation with LPS, however, Piezo1 was upregulated in ~25% of astrocytes and much larger Ca^{2+} influxes were observed (Figure 3a). Moreover, 60% of reactive astrocytes responded to Yoda1 versus 48% of control astrocytes (Figure 3b). Therefore, the predominant component of the Yoda1-mediated Ca^{2+} response in reactive astrocytes is likely regulated by Piezo1 channels, even though a smaller off-target component is also detectable.

Our data also demonstrate that Piezo1-mediated Ca^{2+} influx into LPS-stimulated astrocytes may trigger internal store-driven Ca^{2+} oscillations. In the absence of extracellular Ca^{2+} , Yoda1 induced a net efflux of Ca^{2+} to the extracellular space of control astrocytes. In contrast, Yoda1 caused a net enhancement of cytosolic Ca^{2+} concentration in LPS-reactive astrocytes (Figure 5a). Since Piezo1 expression is almost absent in control astrocytes, Yoda1-mediated efflux of Ca^{2+} may be caused by the nonspecific opening of membrane-bound cation channels (e.g., TRP channels), thus allowing Ca^{2+} to flow out of the cell and into the Ca^{2+} and Mg^{2+} free medium. LPS-reactive astrocytes, on the other hand, upregulate Piezo1 channels (Figure 1) and given that Piezo1 can localize to the ER (Mc Hugh et al., 2010), our data suggests that Yoda1 triggers calcium release from internal stores, possibly via intracellular Piezo1 channels (Figure 8). Moreover, depletion of Ca^{2+} from internal stores can activate calcium release-activated channels (CRAC) in the outer membrane, thus enhancing extracellular Ca^{2+} influx and facilitating the replenishment of internal calcium stores (Prakriya, 2009). Indeed, in the presence of extracellular Ca^{2+} , we found that Yoda1 initially enhances cytosolic Ca^{2+} levels (most likely via Ca^{2+} influx through membrane-bound Piezo1 channels), which in turn has the potential to cause calcium-induced calcium release (CICR) from intracellular stores. CICR can also trigger further Ca^{2+} entry via membrane-expressed store-operated calcium channels (SOCs), such as TRP cation channels, which are expressed both on the outer cell membrane as well as localized to the ER (Dong, Wang, & Xu, 2010; Verkhatsky & Parpura, 2014). Taken together, this could explain why we observed more Ca^{2+} influx 2–4 min post-Yoda1 exposure versus the first 2 min of Yoda1 treatment (Figure 3a).

4.3 | Piezo1 and ATP-responsiveness in astrocytes

Prior activation of Piezo1, with Yoda1, decreased Ca^{2+} influx in response to ATP stimulation. This suggests that Piezo1 activation in

reactive astrocytes could have both local and long-range consequences for neurotransmission in the cerebral cortex. Indeed, paracrine signaling in astrocyte networks is facilitated through ATP-mediated upregulation of inositol trisphosphate (IP_3) which triggers the release of Ca^{2+} from internal stores (Fumagalli et al., 2003; Kastiris, Salm, & McCarthy, 1992), and this, in turn, causes the release of more ATP from the astrocyte. ATP released from astrocytes can activate purinergic (P2X) receptors on the postsynaptic neuron and induce metaplastic changes in synaptic strength (Boue-Grabot & Pankratov, 2017). Bi-directional modulation of glutamatergic synaptic transmission has been demonstrated through either slow and prolonged decreases in AMPA receptor-mediated mini excitatory postsynaptic currents (mEPSCs; Pougnet et al., 2014) or via P2X-mediated insertion of AMPA receptors into the postsynaptic membrane which culminates in the long-term enhancement of mEPSC amplitude (Gordon et al., 2005).

ATP is also important in the propagation of Ca^{2+} waves through astrocyte networks (Fujii, Maekawa, & Morita, 2017). Moreover, vasoactive substance release is regulated by astrocytic Ca^{2+} waves and ATP-induced Ca^{2+} release from intracellular stores within astrocytes (Metea & Newman, 2006). Therefore, astrocyte branches release factors that can induce vasoconstriction or vasodilation of cerebral vasculature (Filosa & Iddings, 2013). Piezo1-mediated dampening of ATP-induced Ca^{2+} waves in astrocytes could, in theory, regulate cerebral blood flow. Indeed, Piezo1 is activated by shear stress, which leads to increases in NOS and NO release from vasculature-derived endothelial cells (Wang et al., 2016). Since astrocytic endfeet are in contact with pericytes that wrap around cerebral blood vessels (Abbott, Ronnback, & Hansson, 2006; Bonkowski, Katyshev, Balabanov, Borisov, & Dore-Duffy, 2011), it would be interesting to study the role of astrocytic Piezo1 in the regulation of vascular tone and blood brain barrier permeability in future experiments.

4.4 | Piezo1 and neuroinflammation

Because astrocytes are also an important source of neuromodulatory cytokine and chemokine production post-LPS exposure (Lieberman, Pitha, Shin, & Shin, 1989; Rothhammer & Quintana, 2015), we measured the effects of Piezo1 activation on IL-1 β , TNF α , IL-6, and CX₃CL1 release from reactive astrocytes. Blocking Piezo1 channels, using GsMTx4, had little or no effect on cytokine release. However, activating Piezo1 channels with Yoda1 significantly decreased pro-inflammatory cytokine release from LPS-stimulated cortical astrocytes. We also found that Yoda1 decreased CX₃CL1 release from unstimulated control astrocytes (Figure 7d). Therefore, the anti-inflammatory effects of Yoda1 may not be entirely dependent on Piezo1 activation. Yoda1 may cause a general dampening of cytokine secretory activity in astrocytes.

Although LPS-induced upregulation of Piezo1 in cultured astrocytes is somewhat transient (Figure 1), with protein levels decreasing again after 48 hr; chronic overexpression of Piezo1 does occur in vivo, particularly in reactive astrocytes surrounding amyloid plaques in the ageing brain of Alzheimer's disease (AD) rats harboring a



chronic urinary tract infection (Velasco-Estevéz et al., 2018). It is interesting to speculate on the potential functional roles of Piezo1, as well as the potential triggers of mechanosensitive channel opening, in the ageing and neurodegenerating brain (Tyler, 2012). We hypothesize that stiff amyloid plaques scattered randomly throughout the AD brain act as extrinsic mechanical modulators of Piezo1 channel opening probability. In addition, Piezo1 activity may be modulated by the gradual softening of ageing AD brain tissue (ElSheikh et al., 2017) which also undergoes extracellular matrix (ECM) remodeling at sub-cellular length scales (Sethi & Zaia, 2017). Moreover, because amyloid plaques represent an altered extrinsic mechanical environment for astrocytes in vivo, Piezo1 ion channels could potentially modulate mechanotransduction signaling in reactive astrocytes in response to amyloid accumulation. Interestingly, Piezo1 regulates the expression of the mechanoresponsive transcriptional cofactor Yes-associated protein (YAP) and activates the Hippo signaling pathway (Pathak et al., 2014) which controls important processes such as cell contact inhibition and cell proliferation (Pavel et al., 2018). YAP is highly expressed by astrocytes and can activate suppressor of cytokine signaling (SOCS), thus preventing astrocyte reactivity by downregulating the JAK-STAT inflammatory pathway (Huang et al., 2016). It will be important in future experiments to investigate the potential anti-inflammatory mechanism of action of astrocytic Piezo1 in more detail and to determine if Piezo1 could be a novel drug target for neuro-inflammatory disorders of the ageing brain.

5 | CONCLUSION

The data presented here suggests that mechanosensitive astrocytes upregulate Piezo1 channels in response to LPS in an attempt to inhibit pro-inflammatory cytokine release and dampen neuroinflammation. Activation of Piezo1 channels with Yoda1 slowed astrocyte migration and blocked TNF α , IL-1 β , and CX₃CL1 release from LPS-stimulated astrocytes. This is likely through Ca²⁺-dependent signaling cascades since Piezo1 activation enhanced both extracellular Ca²⁺ influx and internal store-mediated release of Ca²⁺ into the cytosol of reactive astrocytes. Moreover, Piezo1-mediated Ca²⁺ influx dampens subsequent ATP-induced Ca²⁺ responses in astrocytes, suggesting that Piezo1 could modulate neurotransmission by regulating gliotransmitter release at the synapse. It will be important, going forward, to investigate if there is a link between Ca²⁺-mediated mechanotransduction in astrocytes and other well-known biochemical signaling pathways that regulate synaptic plasticity, particularly in the ageing neuroinflammatory brain.

ACKNOWLEDGMENTS

The authors wish to thank Sinead O'Sullivan for valuable technical assistance in the early stages of the project. This work was supported by an Irish Research Council PhD scholarship to M.V.E., a Crick PhD studentship to S.O.R., a University of Brighton PhD studentship to M. M, and a *Pump Priming* research grant to G.K.S. from the University of

Brighton. G.K.S. is also grateful for funding from the Leverhulme Trust [RPG-2018-443].

CONFLICT OF INTEREST

The authors declare no conflict of interest and no competing financial interest.

AUTHOR CONTRIBUTIONS

G.K.S. and K.K.D. conceived the project and designed the research; M.V.E., M.M., and G.K.S. performed the experiments; M.V.E., S.O.R., and G.K.S. analyzed the data; all authors discussed the results, contributed to the writing of the manuscript, and approved the final version.

ORCID

Kumlesh K. Dev  <https://orcid.org/0000-0003-4274-9119>

Graham K. Sheridan  <https://orcid.org/0000-0002-8493-2651>

REFERENCES

- Abbott, N. J., Ronnback, L., & Hansson, E. (2006). Astrocyte-endothelial interactions at the blood-brain barrier. *Nature Reviews. Neuroscience*, 7(1), 41–53. <https://doi.org/10.1038/nrn1824>
- Adzic, M., Stevanovic, I., Josipovic, N., Laketa, D., Lavrnja, I., Bjelobaba, I. M., ... Nedeljkovic, N. (2017). Extracellular ATP induces graded reactive response of astrocytes and strengthens their antioxidative defense in vitro. *Journal of Neuroscience Research*, 95(4), 1053–1066. <https://doi.org/10.1002/jnr.23950>
- Bal-Price, A., Moneer, Z., & Brown, G. C. (2002). Nitric oxide induces rapid, calcium-dependent release of vesicular glutamate and ATP from cultured rat astrocytes. *Glia*, 40(3), 312–323. <https://doi.org/10.1002/glia.10124>
- Blumenthal, N. R., Hermanson, O., Heimrich, B., & Shastri, V. P. (2014). Stochastic nanoroughness modulates neuron-astrocyte interactions and function via mechanosensing cation channels. *Proceedings of the National Academy of Sciences of the United States of America*, 111(45), 16124–16129. <https://doi.org/10.1073/pnas.1412740111>
- Bonkowski, D., Katyshev, V., Balabanov, R. D., Borisov, A., & Dore-Duffy, P. (2011). The CNS microvascular pericyte: Pericyte-astrocyte crosstalk in the regulation of tissue survival. *Fluids Barriers CNS*, 8(1), 8. <https://doi.org/10.1186/2045-8118-8-8>
- Boue-Grabot, E., & Pankratov, Y. (2017). Modulation of central synapses by astrocyte-released ATP and postsynaptic P2X receptors. *Neural Plasticity*, 2017, 9454275–9454211. <https://doi.org/10.1155/2017/9454275>
- Bowers, H. C., Fiori, M. L., Khadela, J. B., Janmey, P. A., & Galie, P. A. (2019). Cell-matrix tension contributes to hypoxia in astrocyte-seeded viscoelastic hydrogels composed of collagen and hyaluronan. *Experimental Cell Research*, 376(1), 49–57. <https://doi.org/10.1016/j.yexcr.2019.01.012>
- Buffo, A., Rolando, C., & Ceruti, S. (2010). Astrocytes in the damaged brain: Molecular and cellular insights into their reactive response and healing potential. *Biochemical Pharmacology*, 79(2), 77–89. <https://doi.org/10.1016/j.bcp.2009.09.014>
- Cahalan, S. M., Lukacs, V., Ranade, S. S., Chien, S., Bandell, M., & Patapoutian, A. (2015). Piezo1 links mechanical forces to red blood cell volume. *eLife*, 4, e07370. <https://doi.org/10.7554/eLife.07370>

- Cardenas, A., Kong, M., Alvarez, A., Maldonado, H., & Leyton, L. (2014). Signaling pathways involved in neuron-astrocyte adhesion and migration. *Current Molecular Medicine*, 14(2), 275–290.
- Chesnokova, V., Pechnick, R. N., & Wawrowsky, K. (2016). Chronic peripheral inflammation, hippocampal neurogenesis, and behavior. *Brain, Behavior, and Immunity*, 58, 1–8. <https://doi.org/10.1016/j.bbi.2016.01.017>
- Choi, H. J., Sun, D., & Jakobs, T. C. (2015). Astrocytes in the optic nerve head express putative mechanosensitive channels. *Molecular Vision*, 21, 749–766.
- Chubinskiy-Nadezhdin, V. I., Vasileva, V. Y., Vassilieva, I. O., Sudarikova, A. V., Morachevskaya, E. A., & Negulyaev, Y. A. (2019). Agonist-induced Piezo1 activation suppresses migration of transformed fibroblasts. *Biochemical and Biophysical Research Communications*, 514(1), 173–179. <https://doi.org/10.1016/j.bbrc.2019.04.139>
- Copeland, C. S., Wall, T. M., Sims, R. E., Neale, S. A., Nisenbaum, E., Parri, H. R., & Salt, T. E. (2017). Astrocytes modulate thalamic sensory processing via mGlu2 receptor activation. *Neuropharmacology*, 121, 100–110. <https://doi.org/10.1016/j.neuropharm.2017.04.019>
- Dela Paz, N. G., & Frangos, J. A. (2018). Yoda1-induced phosphorylation of Akt and ERK1/2 does not require Piezo1 activation. *Biochemical and Biophysical Research Communications*, 497(1), 220–225. <https://doi.org/10.1016/j.bbrc.2018.02.058>
- Dong, X. P., Wang, X., & Xu, H. (2010). TRP channels of intracellular membranes. *Journal of Neurochemistry*, 113, 313–328. <https://doi.org/10.1111/j.1471-4159.2010.06626.x>
- Eisenhoffer, G. T., Loftus, P. D., Yoshigi, M., Otsuna, H., Chien, C. B., Morcos, P. A., & Rosenblatt, J. (2012). Crowding induces live cell extrusion to maintain homeostatic cell numbers in epithelia. *Nature*, 484(7395), 546–549. <https://doi.org/10.1038/nature10999>
- El-Hage, N., Podhaizer, E. M., Sturgill, J., & Hauser, K. F. (2011). Toll-like receptor expression and activation in astroglia: Differential regulation by HIV-1 Tat, gp120, and morphine. *Immunological Investigations*, 40(5), 498–522. <https://doi.org/10.3109/08820139.2011.561904>
- EISheikh, M., Arani, A., Perry, A., Boeve, B. F., Meyer, F. B., Savica, R., ... Huston, J., 3rd. (2017). MR Elastography demonstrates unique regional brain stiffness patterns in dementias. *AJR. American Journal of Roentgenology*, 209(2), 403–408. <https://doi.org/10.2214/AJR.16.17455>
- Fellin, T., Pascual, O., Gobbo, S., Pozzan, T., Haydon, P. G., & Carmignoto, G. (2004). Neuronal synchrony mediated by astrocytic glutamate through activation of extrasynaptic NMDA receptors. *Neuron*, 43(5), 729–743. <https://doi.org/10.1016/j.neuron.2004.08.011>
- Filosa, J. A., & Iddings, J. A. (2013). Astrocyte regulation of cerebral vascular tone. *American Journal of Physiology. Heart and Circulatory Physiology*, 305(5), H609–H619. <https://doi.org/10.1152/ajpheart.00359.2013>
- Friedl, P., & Brocker, E. B. (2000). The biology of cell locomotion within three-dimensional extracellular matrix. *Cellular and Molecular Life Sciences*, 57(1), 41–64. <https://doi.org/10.1007/s000180050498>
- Fujii, Y., Maekawa, S., & Morita, M. (2017). Astrocyte calcium waves propagate proximally by gap junction and distally by extracellular diffusion of ATP released from volume-regulated anion channels. *Scientific Reports*, 7(1), 13115. <https://doi.org/10.1038/s41598-017-13243-0>
- Fumagalli, M., Brambilla, R., D'Ambrosi, N., Volonte, C., Matteoli, M., Verderio, C., & Abbracchio, M. P. (2003). Nucleotide-mediated calcium signaling in rat cortical astrocytes: Role of P2X and P2Y receptors. *Glia*, 43(3), 218–203. <https://doi.org/10.1002/glia.10248>
- Gordon, G. R., Baimoukhametova, D. V., Hewitt, S. A., Rajapaksha, W. R., Fisher, T. E., & Bains, J. S. (2005). Norepinephrine triggers release of glial ATP to increase postsynaptic efficacy. *Nature Neuroscience*, 8(8), 1078–1086. <https://doi.org/10.1038/nn1498>
- Gottlieb, P. A., & Sachs, F. (2012). Piezo1: Properties of a cation selective mechanical channel. *Channels (Austin, Tex.)*, 6(4), 214–219. <https://doi.org/10.4161/chan.21050>
- Healy, L. M., Sheridan, G. K., Pritchard, A. J., Rutkowska, A., Mullershausen, F., & Dev, K. K. (2013). Pathway specific modulation of S1P1 receptor signalling in rat and human astrocytes. *British Journal of Pharmacology*, 169(5), 1114–1129. <https://doi.org/10.1111/bph.12207>
- Huang, Z., Wang, Y., Hu, G., Zhou, J., Mei, L., & Xiong, W. C. (2016). YAP is a critical inducer of SOCS3, preventing reactive astrogliosis. *Cerebral Cortex*, 26(5), 2299–2310. <https://doi.org/10.1093/cercor/bhv292>
- Hung, W. C., Yang, J. R., Yankaskas, C. L., Wong, B. S., Wu, P. H., Pardo-Pastor, C., ... Konstantopoulos, K. (2016). Confinement sensing and signal optimization via Piezo1/PKA and myosin II pathways. *Cell Reports*, 15(7), 1430–1441. <https://doi.org/10.1016/j.celrep.2016.04.035>
- Jacob, F., Perez Novo, C., Bachert, C., & Van Crombruggen, K. (2013). Purinergic signaling in inflammatory cells: P2 receptor expression, functional effects, and modulation of inflammatory responses. *Purinergic Signal*, 9(3), 285–306. <https://doi.org/10.1007/s11302-013-9357-4>
- Jacques-Fricke, B. T., Seow, Y., Gottlieb, P. A., Sachs, F., & Gomez, T. M. (2006). Ca²⁺ influx through mechanosensitive channels inhibits neurite outgrowth in opposition to other influx pathways and release from intracellular stores. *The Journal of Neuroscience*, 26(21), 5656–5664. <https://doi.org/10.1523/jneurosci.0675-06.2006>
- Kastritsis, C. H., Salm, A. K., & McCarthy, K. (1992). Stimulation of the P2Y purinergic receptor on type 1 astroglia results in inositol phosphate formation and calcium mobilization. *Journal of Neurochemistry*, 58(4), 1277–1284.
- Koser, D. E., Thompson, A. J., Foster, S. K., Dwivedy, A., Pillai, E. K., Sheridan, G. K., ... Franze, K. (2016). Mechanosensing is critical for axon growth in the developing brain. *Nature Neuroscience*, 19(12), 1592–1598. <https://doi.org/10.1038/nn.4394>
- Lacroix, J. J., Botello-Smith, W. M., & Luo, Y. (2018). Probing the gating mechanism of the mechanosensitive channel Piezo1 with the small molecule Yoda1. *Nature Communications*, 9(1), 2029. <https://doi.org/10.1038/s41467-018-04405-3>
- Leybaert, L., & Sanderson, M. J. (2012). Intercellular Ca(2+) waves: Mechanisms and function. *Physiological Reviews*, 92(3), 1359–1392. <https://doi.org/10.1152/physrev.00029.2011>
- Li, C., Rezaei, S., Kammerer, S., Sokolowski, A., Devaney, T., Gorischek, A., ... Schreiber, W. (2015). Piezo1 forms mechanosensitive ion channels in the human MCF-7 breast cancer cell line. *Scientific Reports*, 5, 8364. <https://doi.org/10.1038/srep08364>
- Li, J., Hou, B., Tumova, S., Muraki, K., Bruns, A., Ludlow, M. J., ... Beech, D. J. (2014). Piezo1 integration of vascular architecture with physiological force. *Nature*, 515(7526), 279–282. <https://doi.org/10.1038/nature13701>
- Liddel, S. A., Gattenplan, K. A., Clarke, L. E., Bennett, F. C., Bohlen, C. J., Schirmer, L., ... Barres, B. A. (2017). Neurotoxic reactive astrocytes are induced by activated microglia. *Nature*, 541(7638), 481–487. <https://doi.org/10.1038/nature21029>
- Lieberman, A. P., Pitha, P. M., Shin, H. S., & Shin, M. L. (1989). Production of tumor necrosis factor and other cytokines by astrocytes stimulated with lipopolysaccharide or a neurotropic virus. *Proceedings of the National Academy of Sciences of the United States of America*, 86(16), 6348–6352.
- Liu, C. S. C., Raychaudhuri, D., Paul, B., Chakrabarty, Y., Ghosh, A. R., Rahaman, O., ... Ganguly, D. (2018). Cutting edge: Piezo1 mechanosensors optimize human T cell activation. *Journal of Immunology*, 200(4), 1255–1260. <https://doi.org/10.4049/jimmunol.1701118>
- Maneshi, M. M., Sachs, F., & Hua, S. Z. (2015). A threshold shear force for calcium influx in an astrocyte model of traumatic brain injury. *Journal of Neurotrauma*, 32(13), 1020–1029. <https://doi.org/10.1089/neu.2014.3677>
- Maroto, R., Kurosky, A., & Hamill, O. P. (2012). Mechanosensitive Ca(2+) permeant cation channels in human prostate tumor cells. *Channels (Austin, Tex.)*, 6(4), 290–307. <https://doi.org/10.4161/chan.21063>



- Matias, I., Morgado, J., & Gomes, F. C. A. (2019). Astrocyte heterogeneity: Impact to brain aging and disease. *Frontiers in Aging Neuroscience*, *11*, 59. <https://doi.org/10.3389/fnagi.2019.00059>
- McHugh, B. J., Buttery, R., Lad, Y., Banks, S., Haslett, C., & Sethi, T. (2010). Integrin activation by Fam38A uses a novel mechanism of R-Ras targeting to the endoplasmic reticulum. *Journal of Cell Science*, *123*(Pt 1), 51–61. <https://doi.org/10.1242/jcs.056424>
- McHugh, B. J., Murdoch, A., Haslett, C., & Sethi, T. (2012). Loss of the integrin-activating transmembrane protein Fam38A (Piezo1) promotes a switch to a reduced integrin-dependent mode of cell migration. *PLoS One*, *7*(7), e40346. <https://doi.org/10.1371/journal.pone.0040346>
- Metea, M. R., & Newman, E. A. (2006). Glial cells dilate and constrict blood vessels: A mechanism of neurovascular coupling. *The Journal of Neuroscience*, *26*(11), 2862–2870. <https://doi.org/10.1523/jneurosci.4048-05.2006>
- Moroni, M., Servin-Vences, M. R., Fleischer, R., Sanchez-Carranza, O., & Lewin, G. R. (2018). Voltage gating of mechanosensitive PIEZO channels. *Nature Communications*, *9*(1), 1096. <https://doi.org/10.1038/s41467-018-03502-7>
- Moshayedi, P., Costa Lda, F., Christ, A., Lacour, S. P., Fawcett, J., Guck, J., & Franze, K. (2010). Mechanosensitivity of astrocytes on optimized polyacrylamide gels analyzed by quantitative morphometry. *Journal of Physics: Condensed Matter*, *22*(19), 194114. <https://doi.org/10.1088/0953-8984/22/19/194114>
- Moshayedi, P., Ng, G., Kwok, J. C., Yeo, G. S., Bryant, C. E., Fawcett, J. W., ... Guck, J. (2014). The relationship between glial cell mechanosensitivity and foreign body reactions in the central nervous system. *Biomaterials*, *35*(13), 3919–3925. <https://doi.org/10.1016/j.biomaterials.2014.01.038>
- Nakano, Y., Furube, E., Morita, S., Wanaka, A., Nakashima, T., & Miyata, S. (2015). Astrocytic TLR4 expression and LPS-induced nuclear translocation of STAT3 in the sensory circumventricular organs of adult mouse brain. *Journal of Neuroimmunology*, *278*, 144–158. <https://doi.org/10.1016/j.jneuroim.2014.12.013>
- Nishizaki, T. (2004). ATP- and adenosine-mediated signaling in the central nervous system: Adenosine stimulates glutamate release from astrocytes via A2a adenosine receptors. *Journal of Pharmacological Sciences*, *94*(2), 100–102.
- Nourse, J. L., & Pathak, M. M. (2017). How cells channel their stress: Interplay between Piezo1 and the cytoskeleton. *Seminars in Cell & Developmental Biology*, *71*, 3–12. <https://doi.org/10.1016/j.semcdb.2017.06.018>
- O'Sullivan, S. A., Velasco-Estevéz, M., & Dev, K. K. (2017). Demyelination induced by oxidative stress is regulated by sphingosine 1-phosphate receptors. *Glia*, *65*(7), 1119–1136. <https://doi.org/10.1002/glia.23148>
- Pathak, M. M., Nourse, J. L., Tran, T., Hwe, J., Arulmoli, J., Le, D. T., ... Tombola, F. (2014). Stretch-activated ion channel Piezo1 directs lineage choice in human neural stem cells. *Proceedings of the National Academy of Sciences of the United States of America*, *111*(45), 16148–16153. <https://doi.org/10.1073/pnas.1409802111>
- Pau, G., Fuchs, F., Sklyar, O., Boutros, M., & Huber, W. (2010). EBIImage-- An R package for image processing with applications to cellular phenotypes. *Bioinformatics*, *26*(7), 979–981. <https://doi.org/10.1093/bioinformatics/btq046>
- Pavel, M., Renna, M., Park, S. J., Menzies, F. M., Ricketts, T., Fullgrabe, J., ... Rubinsztein, D. C. (2018). Contact inhibition controls cell survival and proliferation via YAP/TAZ-autophagy axis. *Nature Communications*, *9*(1), 2961. <https://doi.org/10.1038/s41467-018-05388-x>
- Pouget, J. T., Toulme, E., Martinez, A., Choquet, D., Hossy, E., & Boue-Grabot, E. (2014). ATP P2X receptors downregulate AMPA receptor trafficking and postsynaptic efficacy in hippocampal neurons. *Neuron*, *83*(2), 417–430. <https://doi.org/10.1016/j.neuron.2014.06.005>
- Prakriya, M. (2009). The molecular physiology of CRAC channels. *Immunological Reviews*, *231*, 88–98. <https://doi.org/10.1111/j.1600-065X.2009.00820.x>
- Rocha, D. N., Ferraz-Nogueira, J. P., Barrias, C. C., Relvas, J. B., & Pego, A. P. (2015). Extracellular environment contribution to astrogliosis-lessons learned from a tissue engineered 3D model of the glial scar. *Frontiers in Cellular Neuroscience*, *9*, 377. <https://doi.org/10.3389/fncel.2015.00377>
- Rorth, P. (2009). Collective cell migration. *Annual Review of Cell and Developmental Biology*, *25*, 407–429. <https://doi.org/10.1146/annurev.cellbio.042308.113231>
- Rothhammer, V., & Quintana, F. J. (2015). Control of autoimmune CNS inflammation by astrocytes. *Seminars in Immunopathology*, *37*(6), 625–638. <https://doi.org/10.1007/s00281-015-0515-3>
- Scemes, E., & Giaume, C. (2006). Astrocyte calcium waves: What they are and what they do. *Glia*, *54*(7), 716–725. <https://doi.org/10.1002/glia.20374>
- Serrano, A., Haddjeri, N., Lacaillle, J. C., & Robitaille, R. (2006). GABAergic network activation of glial cells underlies hippocampal heterosynaptic depression. *The Journal of Neuroscience*, *26*(20), 5370–5382. <https://doi.org/10.1523/jneurosci.5255-05.2006>
- Sethi, M. K., & Zaia, J. (2017). Extracellular matrix proteomics in schizophrenia and Alzheimer's disease. *Analytical and Bioanalytical Chemistry*, *409*(2), 379–394. <https://doi.org/10.1007/s00216-016-9900-6>
- Simen, A. A., Bordner, K. A., Martin, M. P., Moy, L. A., & Barry, L. C. (2011). Cognitive dysfunction with aging and the role of inflammation. *Therapeutic Advances in Chronic Disease*, *2*(3), 175–195. <https://doi.org/10.1177/2040622311399145>
- Sofroniew, M. V., & Vinters, H. V. (2010). Astrocytes: Biology and pathology. *Acta Neuropathologica*, *119*(1), 7–35. <https://doi.org/10.1007/s00401-009-0619-8>
- Song, Y., Li, D., Farrelly, O., Miles, L., Li, F., Kim, S. E., ... Jan, Y. N. (2019). The mechanosensitive ion channel Piezo inhibits axon regeneration. *Neuron*, *102*(2), 373–389. <https://doi.org/10.1016/j.neuron.2019.01.050>
- Syeda, R., Xu, J., Dubin, A. E., Coste, B., Mathur, J., Huynh, T., ... Patapoutian, A. (2015). Chemical activation of the mechanotransduction channel Piezo1. *eLife*, *4*, e07369. <https://doi.org/10.7554/eLife.07369>
- Tyler, W. J. (2012). The mechanobiology of brain function. *Nature Reviews Neuroscience*, *13*(12), 867–878. <https://doi.org/10.1038/nrn3383>
- Velasco-Estevéz, M., Mampay, M., Boutin, H., Chaney, A., Warn, P., Burgess, E., ... Sheridan, G. K. (2018). Infection augments expression of mechanosensing Piezo1 channels in amyloid plaque-reactive astrocytes. *Frontiers in Aging Neuroscience*, *10*, 332. <https://doi.org/10.3389/fnagi.2018.00332>
- Verkhatsky, A., & Parpura, V. (2014). Store-operated calcium entry in neuroglia. *Neuroscience Bulletin*, *30*, 125–133. <https://doi.org/10.1007/s12264-013-1343-x>
- Wang, S., Chennupati, R., Kaur, H., Iring, A., Wettschreck, N., & Offermanns, S. (2016). Endothelial cation channel PIEZO1 controls blood pressure by mediating flow-induced ATP release. *The Journal of Clinical Investigation*, *126*(12), 4527–4536. <https://doi.org/10.1172/jci87343>
- Yang, X. N., Lu, Y. P., Liu, J. J., Huang, J. K., Liu, Y. P., Xiao, C. X., ... Guleng, B. (2014). Piezo1 is as a novel trefoil factor family 1 binding protein that promotes gastric cancer cell mobility in vitro. *Digestive Diseases and Sciences*, *59*(7), 1428–1435. <https://doi.org/10.1007/s10620-014-3044-3>
- Zhan, J. S., Gao, K., Chai, R. C., Jia, X. H., Luo, D. P., Ge, G., ... Yu, A. C. (2017). Astrocytes in migration. *Neurochemical Research*, *42*(1), 272–282. <https://doi.org/10.1007/s11064-016-2089-4>

How to cite this article: Velasco-Estevéz M, Rolle SO, Mampay M, Dev KK, Sheridan GK. Piezo1 regulates calcium oscillations and cytokine release from astrocytes. *Glia*. 2020; 68:145–160. <https://doi.org/10.1002/glia.23709>